

Measurement of the Chiral-Odd Generalized Parton Distribution Functions and Non-Parametric Analysis of the Deeply Virtual Neutral Pion Electroproduction Cross Section at the Thomas Jefferson National Accelerator Facility at 10.6 GeV

by

Robert Johnston

Submitted to the Department of Physics
in partial fulfillment of the requirements for the degree of

Interdisciplinary PhD in Physics and Statistics

at the

MASSACHUSETTS INSTITUTE OF TECHNOLOGY

June 2023

© Massachusetts Institute of Technology 2023. All rights reserved.

Author Department of Physics
May 5, 2023

Certified by..... Richard Milner
Professor of Physics
Thesis Supervisor

Accepted by Lindley Winslow
Associate Department Head of Physics

**Measurement of the Chiral-Odd Generalized Parton
Distribution Functions and Non-Parametric Analysis of the
Deeply Virtual Neutral Pion Electroproduction Cross
Section at the Thomas Jefferson National Accelerator
Facility at 10.6 GeV**

by

Robert Johnston

Submitted to the Department of Physics
on May 5, 2023, in partial fulfillment of the
requirements for the degree of
Interdisciplinary PhD in Physics and Statistics

Abstract

Deeply virtual exclusive reactions provide unique channels to study both transverse and longitudinal properties of the nucleon simultaneously, allowing for a 3D image of nucleon substructure. This presentation will discuss work towards extracting an absolute cross section for one such exclusive process, deeply virtual neutral pion production, using 10.6 GeV electron scattering data off a proton target from the CLAS12 experiment in Jefferson Lab Hall B . This measurement is important as exclusive meson production has unique access to the chiral odd GPDs, and is also a background for other exclusive processes such as DVCS, making the determination of this cross section crucial for other exclusive analyses.

Thesis Supervisor: Richard Milner
Title: Professor of Physics

Acknowledgments

To Be Completed. Currently this will serve as a to-do list:

input list of figures

input list of tables

Contents

List of Figures	10
1 Introduction	11
1.1 Background - Structure of the Proton	11
1.2 Deeply Virtual Neutral Pion Production	11
1.2.1 The Handbag Approach	11
1.2.2 The Goloskokov-Kroll Model	11
1.2.3 Status of Measurements	11
1.2.4 Analysis Overview	11
2 Lepton (electron) Scattering	13
2.1 Overview	13
2.2 Quasi-Elastic	14
3 Elastic Scattering	15
3.1 Elastic Low Energy (Proton = Point) Limit: Rutherford and Mott Scattering	15
3.1.1 Rutherford scattering	16
3.1.2 Mott Scattering	17
3.1.3 Summary	17
3.2 Form Factors: Accounting for Proton Structure	17
3.3 Relativistic Electron Proton Elastic Scattering	18
3.3.1 Important Notes	19

3.4	Rosenbluth	20
3.4.1	Rosenbluth Separation - Measuring G_E and G_M	21
3.4.2	Rosenbluth Method Walk through	21
3.5	Olympus and TPEX	23
4	Inelastic Scattering	25
4.1	Overview	25
4.2	Variables	25
4.2.1	Bjorken X	25
4.2.2	Y	26
4.2.3	Q^2	26
4.2.4	W	27
4.3	Deep Inelastic Scattering	27
4.4	Bjorken Scaling and Callan Gross	27
4.5	Structure Functions and Parton Distribution Functions	28
4.6	Scaling and Violations	31
5	Jefferson Lab and CLAS12 Experimental Setup	35
5.1	JLab 12 GeV CEBAF Machine	35
5.1.1	Injector	35
5.1.2	Accelerator and Beam Structure	35
5.1.3	Other notes and comparison to CERN	35
6	Other Halls	37
6.1	Hall A	38
6.1.1	General Layout	38
6.1.2	Tritium Experiment Notes	38
6.1.3	BDX	38
6.1.4	DVCS and DVMP Notes	38
6.2	Hall C	38
6.2.1	Who Cares	38

6.3	Hall D	38
6.3.1	Overview	38
6.3.2	Photon Beam Production and Structure	39
6.3.3	polarization measurement - triplet spectrometers?	40
6.3.4	GlueX Detector Specifications	40
6.3.5	Example Experiment: Charge Pion Polarizability	41
7	CLAS12 System	45
7.1	Overview	45
7.1.1	Introduction	45
7.2	Target and Other	47
7.2.1	Beam from JLab	47
7.2.2	Liquid Hydrogen Target	47
7.2.3	Luminosity Measurement	47
7.2.4	Moller Polarimeters	48
7.2.5	Trigger	51
7.2.6	Faraday Cup	51
7.3	Central Detector	51
7.3.1	SVT	51
7.3.2	MMVT	52
7.3.3	CTOF	54
7.3.4	CND	55
7.3.5	Solenoid	56
7.4	Forward Detector	56
7.4.1	HTCC	56
7.4.2	Torus	58
7.4.3	Drift Chambers	59
7.4.4	LTCC	62
7.4.5	RICH	62
7.4.6	FTOF	65

7.4.7	PCal and ECal	68
8	DVEP and GPDs - what are we here for	75
8.1	GPDs	76
8.1.1	PDFs	76
8.1.2	The GTMD Cube	76
8.1.3	GPDs and Helicity Odd Structure Functions	76
8.2	DVEP	76
8.2.1	DVEP, DVCS, and DVMP	76
8.2.2	How DVPiP Relates to GPDs	76
8.2.3	CLAS12 - DVMP Questions	76
9	Thesis Goal	81
9.1	What do we want at the end of the day and why?	81
10	Analysis Scheme	83
10.1	Preliminary Plots	83
10.1.1	Basic Kinematics	83
10.1.2	DVPP Kinematics	83
10.2	Technical Details	83
10.2.1	Groovy, Python, g/Root, and more	83
10.3	Proton Spin Puzzle	84
10.3.1	Puzzle Origin	84
11	Experimental Setup	85
11.1	Experiment Overview	85
11.2	Accelerator Beamline	85
11.2.1	Overview of Jefferson Lab	85
11.2.2	Electron Source	85
11.2.3	Polarimeters	85
11.2.4	Accelerator	85
11.2.5	Target	85

11.3 CEBAF Large Acceptance Spectrometer	85
11.3.1 Forward Detector	85
11.3.2 Central Detector	85
11.4 Experiment Running and Data Taking	85
12 Simulations	87
12.1 Simulation Infrastructure	87
12.1.1 Motivation for massive simulations	87
12.1.2 OSG, MIT Tier 2, submission pipeline	87
12.2 Generator Details	87
12.2.1 AAO	87
12.2.2 AAONORAD	87
12.2.3 AAORAD	87
12.3 Simulation Pipeline	87
12.4 GEMC	87
12.5 Investigation into Simulation Speedup: Normalizing Flows	87
13 Cross Section Measurement	89
13.1 General Analysis Overview	90
13.2 Data Pre-Processing	90
13.2.1 Energy Loss Corrections	90
13.2.2 Momentum Corrections	90
13.2.3 Simulation:Experiment Resolution Matching	90
13.3 Particle Identification	90
13.4 Event Selection	90
13.4.1 Rigid Event Selection	90
13.4.2 Classifier Based Event Selection	90
13.5 Luminosity	90
13.6 Configuration and Kinematics	90
13.7 Binning	90
13.8 Acceptance Correction	90

13.9 Radiative Corrections	90
13.10 Binning Corrections	90
13.11 Overall Normalization Corrections	90
13.12 Error Analysis	90
14 Further Analysis	91
14.1 Structure Function Extraction	91
14.2 Comparison with CLAS6 Data	91
14.3 T dependence of Slope	91
14.4 Rosenbluth Separation Between Beam Energies	91
14.5 Nonparametric Methods: OMNIFOLD	91
14.6 Conclusion	91
References	93
A	95
A.1 Full Cross Section Data	95
B	97
B.1 Cross check between Andrey Kim and Bobby Johnston	97

Chapter 1

Introduction

1.1 Background - Structure of the Proton

Understanding the structure of matter has been a fundamental research pursuit for centuries.

Proton not a point mass - it has structure

1.2 Deeply Virtual Neutral Pion Production

1.2.1 The Handbag Approach

1.2.2 The Goloskokov-Kroll Model

1.2.3 Status of Measurements

1.2.4 Analysis Overview

Hi ([Bedlinskiy et al., 2014](#)) see more in section [1.1](#) just a test

Chapter 2

Lepton (electron) Scattering

2.1 Overview

We can probe the structure of sub-atomic particles by shooting high energy particles at them. The higher the energy, the shorter distances we resolve. This was done for example in the early 1900s with Rutherford scattering, leading to the discovery of the nucleus in the atom.

For probing the structure of the proton, ideal scattering particles are leptons, as they are point particles with (apparently) no sub-structure themselves. Electrons are the simplest to use as they are stable and easy to produce, but muons and neutrinos are also used.

A key concept is that increasing the energy of the incident particle allows you to resolve shorter distances, which corresponds to different scattering cross sections as you change energy. The following plot illustrates this and is essential:

(e,e'): Energy transfer defines physics

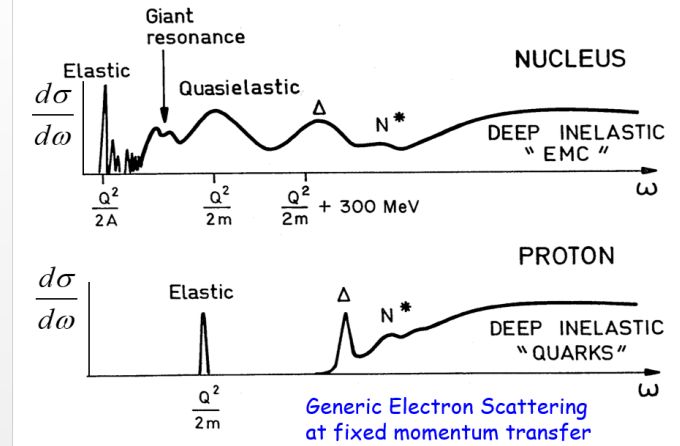


Figure 2-1: Electron-proton scattering cross section vs. energy transfer ω

2.2 Quasi-Elastic

Quasielastic – is broadened due to fermi motion, also slightly shifted due to binding energy of nucleon in nucleus.

Chapter 3

Elastic Scattering

3.1 Elastic Low Energy (Proton = Point) Limit: Rutherford and Mott Scattering

Both Rutherford and Mott scattering neglect the proton recoil and treat the proton as a point source.

The Feynman calculations for this process are straightforward and carried through exactly in Thomson 7.2.

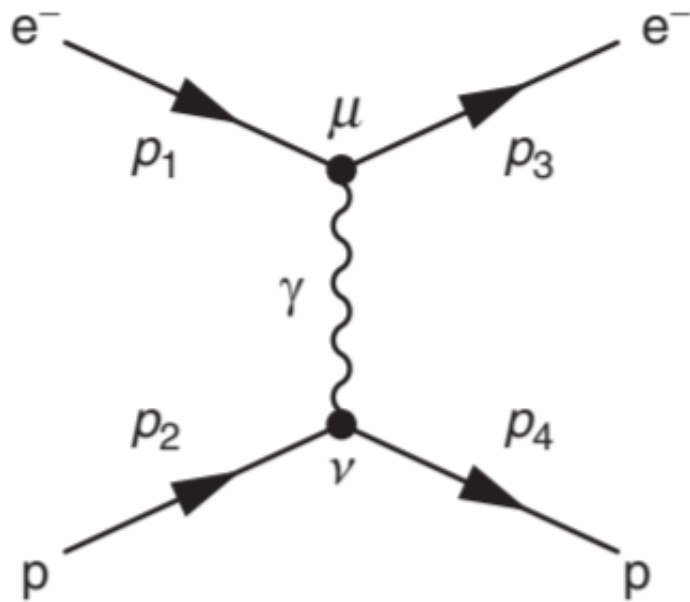


Figure 3-1: Diagram for basic ep scattering

$$\mathcal{M}_{fi} = \frac{Q_q e^2}{q^2} [\bar{u}(p_3)\gamma^\mu u(p_1)] g_{\mu\nu} [\bar{u}(p_4)\gamma^\nu u(p_2)].$$

Figure 3-2: Matrix element for ep scattering

$$\langle|\mathcal{M}_{fi}^2|\rangle = \frac{m_p^2 m_e^2 e^4}{p^4 \sin^4(\theta/2)} \left[1 + \beta_e^2 \gamma_e^2 \cos^2 \frac{\theta}{2} \right].$$

Figure 3-3: Result of matrix element calculation

3.1.1 Rutherford scattering

Rutherford scattering assumes the electron is non-relativistic, yielding a cross section of:

$$\frac{d\sigma}{d\Omega} = \frac{\alpha^2}{16 E_K^2 \sin^4(\theta/2)} \quad (3.1)$$

In this non-relativistic limit, only the interaction between the electric charges of the electron and proton contribute; there is no magnetic (spin-spin) interaction. The angular dependence originates only from the $1/q^2$ propagator term.

3.1.2 Mott Scattering

Mott scattering has a relativistic electron but still fixed point proton. Now since electron momentum is about equal to its energy, reductions lead to the Mott cross section:

$$\frac{d\sigma}{d\Omega} = \frac{\alpha^2}{4E^2 \sin^4(\theta/2)} \cos^2 \frac{\theta}{2} = \left(\frac{\alpha}{2E \sin^2(\theta/2)} \cos \frac{\theta}{2} \right)^2 \quad (3.2)$$

Again, purely magnetic spin-spin interactions are negligible here.

3.1.3 Summary

Rutherford - elastic scattering, proton = fixed, point, electron \neq relativistic

Mott - elastic scattering, proton = fixed, point, electron = relativistic

$$\left(\frac{d\sigma}{d\Omega} \right)_{Mott} = 4 \cos^2 \frac{\theta}{2} \left(\frac{d\sigma}{d\Omega} \right)_{Ruth} \quad (3.3)$$

3.2 Form Factors: Accounting for Proton Structure

If the proton were a point, then the Mott Scattering cross section would agree with experiment for all electron scattering energies. Instead, deviations from Mott are observed as we increase the beam energy. To account for this structure, we need to define form factors, which describe the structure of the proton:

$$\frac{d\sigma}{d\Omega} = \frac{\alpha^2}{4E^2 \sin^4(\theta/2)} \cos^2 \frac{\theta}{2} (F(\mathbf{q}^2))^2 \quad (3.4)$$

$F(\mathbf{q}^2)$ is the 3D Fourier transform of the charge distribution:

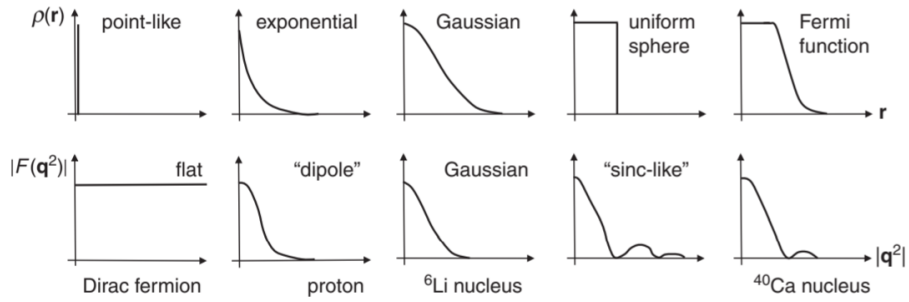


Fig. 7.5

Possible three-dimensional charge distributions and the corresponding form factors plotted as a function of \mathbf{q}^2 .

Figure 3-4: Charge Distribution Fourier Transforms

In general, a spin S particle will have $2S + 1$ form factors. For example, a proton is spin 1/2, and has 2 form factors. A spin 3/2 particle will have 4 form factor (e.g. Li7)

3.3 Relativistic Electron Proton Elastic Scattering

Explicit math is worked out in Thomson 7.4 and is straightforward, but important relations are:

$$\begin{aligned} p_1 &= (E_1, 0, 0, E_1), \\ p_2 &= (m_p, 0, 0, 0), \\ p_3 &= (E_3, 0, E_3 \sin \theta, E_3 \cos \theta), \\ p_4 &= (E_4, \mathbf{p}_4). \end{aligned}$$

Figure 3-5: Kinematic 4-vectors of particle momentum

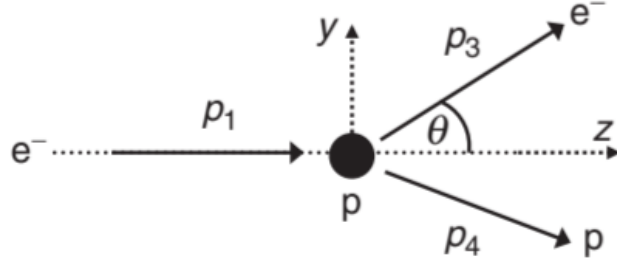


Figure 3-6: Elastic scattering diagram

From the electron - photon - electron vertex, we get the four-momentum squared of the virtual photon (neglect the mass of the electron) q^2 :

$$Q^2 = -q^2 = 4E_1 E_3 \sin^2\left(\frac{\theta}{2}\right) \quad (3.5)$$

We can E_3 expressed in terms of the scattering angle of the electron:

$$E_3 = \frac{E_1 m_p}{m_p + E_1(1 - \cos \theta)} \quad (3.6)$$

This lets us rewrite Q^2 as:

$$Q^2 = \frac{2m_p E_1^2 (1 - \cos \theta)}{m_p + E_1(1 - \cos \theta)} \quad (3.7)$$

Which gives us the differential cross section for the scattering of relativistic electrons from a pointlike proton as:

$$\frac{d\sigma}{d\Omega} = \frac{\alpha^2}{4E_1^2 \sin^4(\theta/2)} \frac{E_3}{E_1} \left(\cos^2 \frac{\theta}{2} + \frac{Q^2}{2m_p^2} \sin^2\left(\frac{\theta}{2}\right) \right) \quad (3.8)$$

3.3.1 Important Notes

Elastic ep scattering has only 1 independent variable, so measuring the scattering angle determines all of the kinematics. In practice, by measuring the energy and angle of scattered electrons, the system can be over constrained to ensure that the scattering was in fact elastic.

Compared to Mott Scattering, there are two differences in the elastic scattering formula. The E_3/E_1 term in the scattering cross section comes from the electron losing energy to the proton's final state kinetic energy (no longer a fixed source). The new term proportional to $\sin^2(\theta/2)$ is due to a purely magnetic spin-spin interaction.

3.4 Rosenbluth

The derived cross-section for elastic scattering still lacks any proton structure. To incorporate structure, we need to include two form factors, $G_E(Q^2)$ - related to the distribution of charge, and $G_M(Q^2)$, related to the distribution of the magnetic moment inside the proton. In the low- Q^2 limit, these form factors are the Fourier transforms of the charge and magnetic moment distributions, but the carryover is not exact in general due to being functions of the 4-momenta, instead of 3 momenta. E.g.:

$$G_E(Q^2) \approx G_E(\mathbf{q}^2) = \int e^{i\mathbf{q}\cdot\mathbf{r}} \rho(\mathbf{r}) d^3\mathbf{r},$$

$$G_M(Q^2) \approx G_M(\mathbf{q}^2) = \int e^{i\mathbf{q}\cdot\mathbf{r}} \mu(\mathbf{r}) d^3\mathbf{r}.$$

Figure 3-7: Interpretations of G_E and G_M

Including these form factors in our cross section gives us the full elastic scattering cross section:

$$\frac{d\sigma}{d\Omega} = \frac{\alpha^2}{4E_1^2 \sin^4(\theta/2)} \frac{E_3}{E_1} \left(\frac{G_E^2 + \tau G_M^2}{1 + \tau} \cos^2 \frac{\theta}{2} + 2\tau G_M^2 \frac{Q^2}{2m_p^2} \sin^2 \left(\frac{\theta}{2} \right) \right) \quad (3.9)$$

Here τ is:

$$\tau = \frac{Q^2}{4m_p^2} \quad (3.10)$$

3.4.1 Rosenbluth Separation - Measuring G_E and G_M

By increasing our beam energy, we will see deviations away from Mott scattering behaviour. We see this explicitly by rewriting the scattering formula as:

$$\frac{d\sigma}{d\Omega} = \left(\frac{G_E^2 + \tau G_M^2}{1 + \tau} + 2\tau G_M^2 \tan^2\left(\frac{\theta}{2}\right) \right) \left(\frac{d\sigma}{d\Omega_0} \right) \quad (3.11)$$

Where $\frac{d\sigma}{d\Omega_0}$ is the Mott Scattering cross section, with the factor of $\frac{E_3}{E_1}$ included to account for proton recoil. We can then extract G_E and G_M in the following way ("Rosenbluth Separation"):

3.4.2 Rosenbluth Method Walk through

Take Data

1.) Experimental set up - electron beam scattering off of proton target. Could use something like GaAs source, Linac up to 0.1 - 1 GeV, incident on proton target, liquid hydrogen should be fine. For a detector, use a dipole spectrometer with scintillating tile focal plane, or something else to measure position well (MWPC, (cheap) silicon strips (expensive, good resolution)). You want to measure the electrons energy so you know E_3 , e.g. you want to be able to over constrain the event so you know it was in fact elastic. Other than that you are just counting events.

2.) Put spectrometer at 135 degrees in theta from the beam axis. Take data at 10 different beam energies. You know know the cross section at that angle at that energy. Now move the spectrometer to 120 degrees. Repeat energy scan. Repeat this process for several other beam angles. You are done taking data.

Analyze data

1.) Go into your data. Using the relation between Q^2 , θ , and E_1 , pick a value of Q^2 (e.g. 0.292 GeV 2 , invert to find the beam energy at the appropriate θ , and note the

cross section at that point. What you just did is find the cross-section value at that angle, corresponding to a specific Q^2 value. Repeat for all the angles you had your spectrometer at. You now have a plot of cross section vs. angle ($\tan(\theta^2)$ so that it is a line), at a specific Q^2 value.

- 2.) Now fit a line to the data. The slope gives you G_M at that Q^2 , and the y-intercept gives you G_E at that Q^2 (see)
- 3.) Repeat steps 1 and 2 for as big of a Q^2 range that you can.

Side notes from Axel - the Rosenbluth method has awful systematics - need to measure absolute cross sections, radiative corrections become large, uncertainties for G_E and G_M are correlated, etc.

Results

Carrying out this procedure gives you plots of G_E and G_M vs. Q^2 .

We see as Q^2 goes to zero, we recover $G_E = 1$ and $G_M = 2.79$, as it should. The data fits well to the so called "dipole function" i.e.:

$$G_M(Q^2) = 2.79 G_E(Q^2) \approx 2.79 \frac{1}{(1 + Q^2/0.71 \text{ GeV}^2)^2}.$$

Figure 3-8: Rosenbluth Results

This relates to a proton charge distribution as exponentially falling off, i.e.

$$\rho(r) \sim \rho_0 e^{-r/a}$$

Here $a = 0.24$ fm, which corresponds to a proton RMS charge radius of 0.8 fm.

Finally, at high Q^2 , $G_M \propto Q^{-4}$, which means that the elastic scattering cross section falls as $1/Q^6$. Also, we can calculate the RMS charge radius of the proton as:

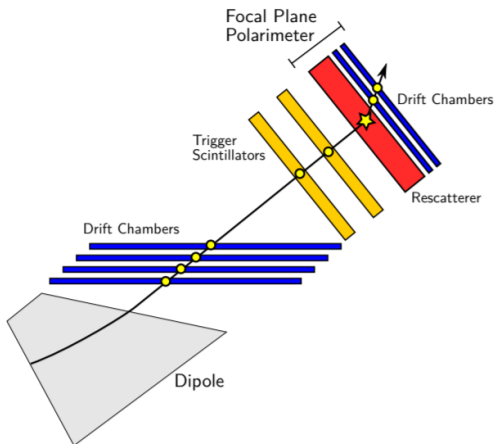
$$\left[-6 \frac{dG_E^p(Q^2)}{dQ^2} \right]_{Q^2=0} \equiv (r_{E,p}^{\text{scatt}})^2.$$

Figure 3-9: Taylor expansion of G_E to yield proton charge radius

3.5 Olympus and TPEX

The Rosenbluth method of measuring the ratio of G_E and G_M has awful systematics, based mainly in the facts that you need to measure an absolute cross section, worry about radiative corrections, and measure at low Q^2 . A better way to measure the proton form factor ratio is by a **polarization transfer** measurement. This uses a **Focal Plane Polarimeter** to convert transverse polarization into an azimuthal distribution:

Polarization can be measured with a focal plane polarimeter.



60

Figure 3-10: Olympus experimental setup

This method has the advantages that we are measuring a ratio, not an absolute cross section, so many uncertainties cancel, such as the FPP analyzing power. Olympus produced the following:

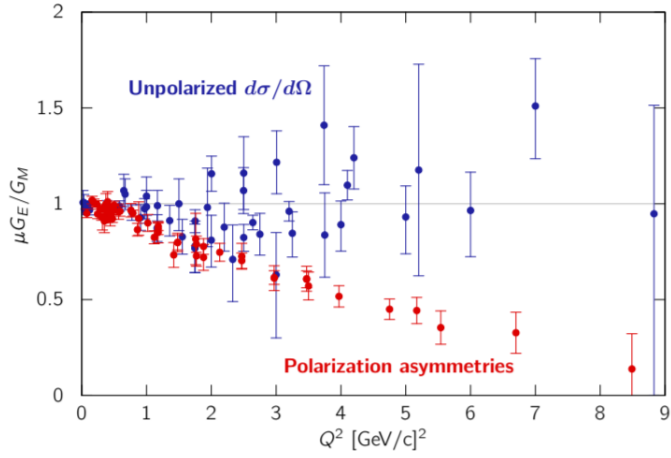


Figure 3-11: G_E and G_M ratio measurements

This discrepancy may be due to two photon exchange, which we can measure by comparing electron to positron scattering:

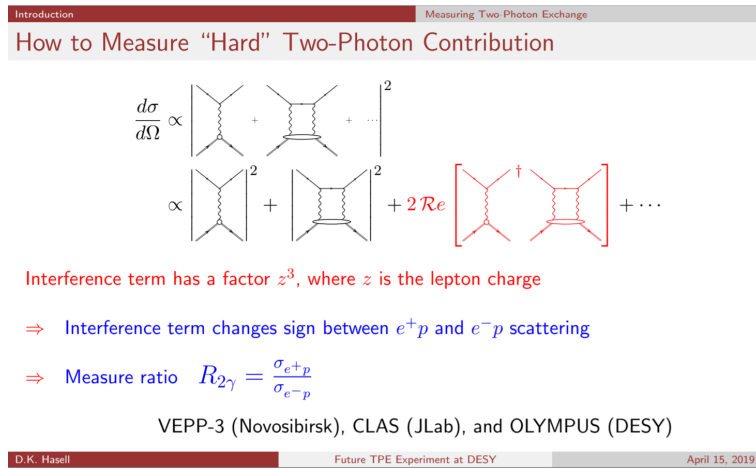


Figure 3-12: Electron Positron charge interference

TPEX is a currently proposed experiment to extend this out to farther Q^2 , which is challenging due to its lower luminosity of elastic scattering as Q^2 increases.

Chapter 4

Inelastic Scattering

4.1 Overview

In inelastic scattering, we now no longer require that the proton remains intact, and we can create resonances, or as we increase the energy, can create a slew of hadronic final states. Since we remove the constraint that the mass of the final state is the proton mass, we now have one extra degree of freedom, i.e., we need 2 variables to describe inelastic scattering. These are usually Bjorken X x_B and the 4-momentum transfer of the virtual photon Q^2 .

N.B. - 1990 Nobel Prize awarded to Friedman, Kendall, and Taylor "for their pioneering investigations concerning deep inelastic scattering of electrons on protons and bound neutrons, which have been of essential importance for the development of the quark model in particle physics"

4.2 Variables

4.2.1 Bjorken X

Think of X_B as the ratio of momentum transfer to energy transfer.

x_B is a measure of elasticity - 1 for elastic scattering. Also, is the fraction of

proton momentum carried by the struck quark in the infinite momentum frame.

$$x = \frac{Q^2}{2p_2 \cdot q} = \frac{Q^2}{Q^2 + W^2 - m_p^2} \quad (4.1)$$

Derivation of infinite momentum frame Bjorken x. Take quark to have momentum fraction ξ of proton's total momentum, i.e. $p_q = \xi p_2$:

Inf. Mom. frame - neglect proton mass so $p_2 = E_2$, neglect all transverse momenta:

Struck quark 4-momenta: $p_q = \xi p_2 = (\xi E_2, \xi E_2, 0, 0)$

4-momenta of quark after interaction: $(p_q + q) = (\xi p_2 + q)$

Square the 4-momenta $(\xi p_2 + q)^2 = \xi^2 p_2^2 + q^2 + 2\xi p_2 \cdot q = m_q^2$

Continue, noting $p_q = \xi p_2$: $m_q^2 = p_q^2 - Q^2 + 2\xi p_2 \cdot q$

Since $p_q^2 = m_q^2$, we have: $m_q^2 = m_q^2 - Q^2 + 2\xi p_2 \cdot q$

So $0 = -Q^2 + 2\xi p_2 \cdot q \longrightarrow \xi = \frac{Q^2}{2p_2 \cdot q} = x_B$

4.2.2 Y

y is a measure of the inelasticity of the scattering, it is the fractional energy lost by the electron in the scattering process (second equality is true where proton is at rest). 0 is for perfectly elastic, 1 is for entirely inelastic.

$$y = \frac{p_2 \cdot q}{p_2 \cdot p_1} = 1 - \frac{E_3}{E_1} \quad (4.2)$$

4.2.3 Q2

With these variables, we can make the equality for Q^2 :

$$Q^2 = (s - m_p^2)xy \sim sxy \quad (4.3)$$

Since you are now breaking up the proton, you have an additional degree of freedom, so you need two observables to describe inelastic scattering.

4.2.4 \mathbf{W}

\mathbf{W} is the four momenta of the final state system that started with the proton, $\mathbf{W} = \mathbf{q} + \mathbf{p}_2$. It is useful as $W^2 = m_p^2 - Q^2 + 2\mathbf{p}_2 \cdot \mathbf{q}$

4.3 Deep Inelastic Scattering

To describe further proton sub-structure, we need to introduce structure functions, $F_1(x, Q^2)$ - purely magnetic, and $F_2(x, Q^2)$. For DIS where $Q^2 \gg m_p^2 y^2$, we have the following cross section formula:

$$\frac{d^2\sigma}{dx dQ^2} \approx \frac{4\pi\alpha^2}{Q^4} \left[(1-y) \frac{F_2(x, Q^2)}{x} + y^2 F_1(x, Q^2) \right].$$

Figure 4-1: General DIS cross section

4.4 Bjorken Scaling and Callan Gross

In DIS, we observe Bjorken scaling and Callan-Gross

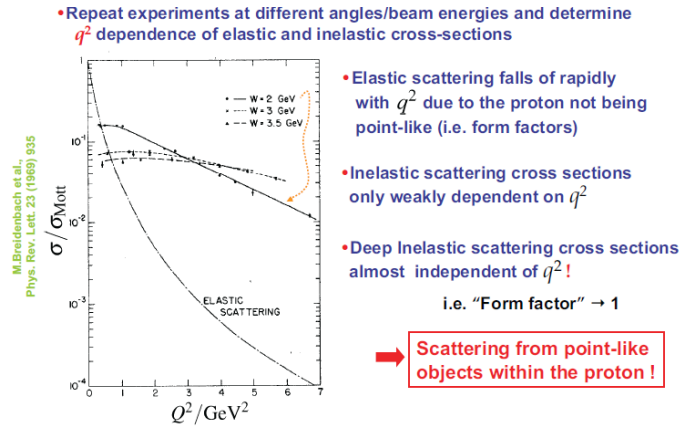


Figure 4-2: Early Bjorken Scaling Example

After performing DIS measurements at SLAC with electron energies between 5 and 20 GeV on liquid hydrogen, using a movable spectrometer over various angles,

showed two important results:

Bjorken Scaling where F_1 and F_2 are basically flat with respect to Q^2 , and thus are independent of Q^2 , indicating that we are scattering off point-like constituents inside the proton.

Callan Gross Relation where $F_2 = 2xF_1$, a relation which can be explained by assuming the underlying process is actually elastic scattering off of point-like spin-half constituents inside the proton (quarks).

4.5 Structure Functions and Parton Distribution Functions

These describe the distribution of quarks within the nucleon. Describes the momentum fraction distribution of quarks. For example:

$$u^p(x)dx$$

Represents the number of up-quarks within the proton with momentum fraction between x and dx . The functional forms of the PDFs are not a-priori known. Some potential PDFs could be as shown below:

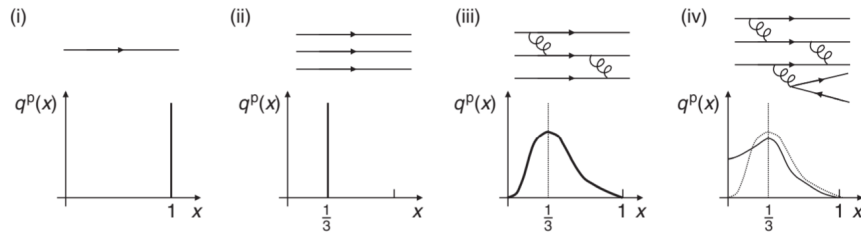


Figure 4-3: Potential PDFs

(i) - if the proton consisted of a single quark

- (ii) - if the proton had 3 static quarks
- (iii) - quarks interacting and Heisenberg uncertainty (momentum smearing)
- (iv) - interacting quarks with higher order diagrams - gluons produced, so enhances low x part of PDF

We can access these distributions experimentally as the parton model predicts the cross section for elastic scattering off of quarks with charge Q_i and momentum fraction in the range of x to $x + dx$ as:

$$\frac{d^2\sigma}{dQ^2} = \frac{4\pi\alpha^2}{Q^4} \left[(1-y) + \frac{y^2}{2} \right] \times Q_i^2 q_i^p(x) \delta x,$$

Figure 4-4: Quark scattering cross section

So then the cross section summing over all quark flavours is:

$$\frac{d^2\sigma^{ep}}{dx dQ^2} = \frac{4\pi\alpha^2}{Q^4} \left[(1-y) + \frac{y^2}{2} \right] \sum_i Q_i^2 q_i^p(x).$$

Figure 4-5: Quark PDF - cross section relation

and comparing it with the general expression for DIS cross section:

$$\frac{d^2\sigma}{dx dQ^2} = \frac{4\pi\alpha^2}{Q^4} \left[(1-y) \frac{F_2^{ep}(x, Q^2)}{x} + y^2 F_1^{ep}(x, Q^2) \right],$$

Figure 4-6: General DIS cross section

We see we can get the relation:

$$F_2^{ep}(x, Q^2) = 2xF_1^{ep}(x, Q^2) = x \sum_i Q_i^2 q_i^p(x).$$

Figure 4-7: Structure function - quark PDF relatio

For an explicit example, we have (neglecting heavier quarks, which have smaller contributions):

$$F_2^{\text{ep}}(x) = x \sum_i Q_i^2 q_i^p(x) \approx x \left(\frac{4}{9} u^p(x) + \frac{1}{9} d^p(x) + \frac{4}{9} \bar{u}^p(x) + \frac{1}{9} \bar{d}^p(x) \right),$$

Figure 4-8: Up and Down quark contributions to structure functions

Note that the parton model predicts both Bjorken scaling and the Callan Gross relation. Importantly, because QCD is hard, the PDFs cannot be calculated from perturbation theory, and must be measured in DIS. We can integrate the PDFs to determine the total momentum fraction of the proton carried by each flavour of quark, as:

$$f_u = \int_0^1 [xu(x) + x\bar{u}(x)] dx \quad \text{and} \quad f_d = \int_0^1 [xd(x) + x\bar{d}(x)] dx.$$

Figure 4-9: Total quark momentum fractions

Doing this after DIS measurements yields $f_u = 0.36$ and $f_d = 0.18$, so the u and d quarks only carry about half of the total momentum of the proton. The rest is carried by gluons, which do not interact in QED ep scattering.

There are other predictions to be made here, such as the ratio of F_2 in neutrons vs. in protons. It would be expected that the ratio would go to 1 as x_B goes to 0, as at low x the PDF is dominated by sea quarks and gluons, which are independent of nucleon type. At high Q^2 we would expect some ratio as basically the number of up quarks to down quarks, but this is not what is seen; instead we observe a modification which might be explained by the fact that it is more likely to have one up quark at high momentum, as if the one down quark were at high momentum, the two up quarks would be closer in phase space, which is disfavoured by the Pauli Exclusion principle.

4.6 Scaling and Violations

Structure functions were studied in great detail (one million DIS events at Q^2 greater than 200 GeV 2 - kinematic range was up to $Q^2 = 20,000 \text{GeV}^2$ and $x < 0.0001$. Q^2 and x were determined solely by precisely measuring the scattering angle and energy of the electron.

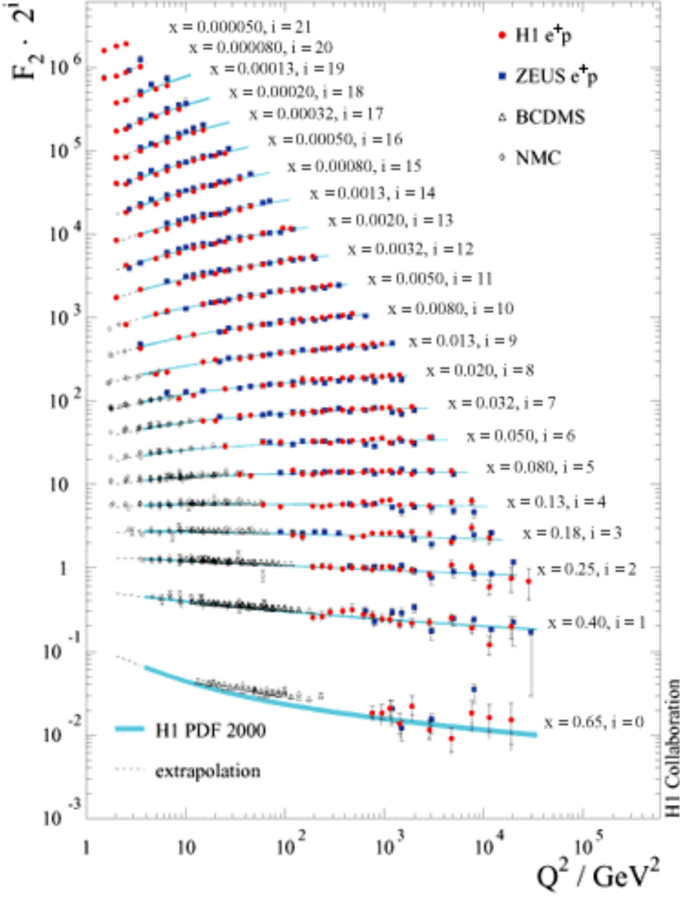


FIG. 2: Structure function F_2 as a function of Q^2 based on HERA-I measurements of H1 [2, 3] and ZEUS [4] collaboration compared to results from fixed target experiments BCDMS [5] and NMC [6].

Figure 4-10: HERA structure functions

2 important takeaways:

1- Bjorken scaling holds up to $Q^2 = 20,000 \text{GeV}^2$, implying that quarks are point like

up to scales of at least 10^{-18}m .

2- Scaling violations:

At medium X , we are independent of Q^2 , indicating we have quarks. At high x , the F_2 structure function decreases at high x , and increases at low x , with increasing Q^2 . More specifically, imagine measuring the F_2 structure function across x at a certain Q^2 . Now measure again at a higher Q^2 . You will see the curve is shifted higher at low x , and lower at high x :

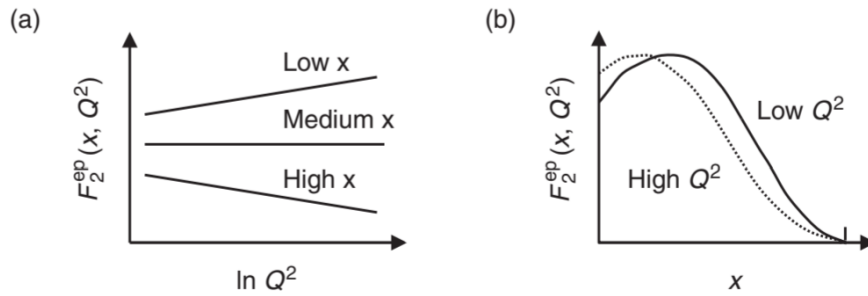


Figure 4-11: Explaination of Scaling Violations

This is indicative of the fact that at higher Q^2 , the proton has a greater fraction of low x quarks. I.e., at low Q^2 we do not "see" the low- x quarks, but as we increase our resolving power, we do.

N.b. - we cannot measure the gluon PDFs, but can model them with QCD parton evolution equations such as DGLAP or BFKL.

Finally, we include a proton PDF at $Q^2 = 10 \text{ GeV}^2$ and at 10^4 GeV^2 . (note - on a semilog plot!)

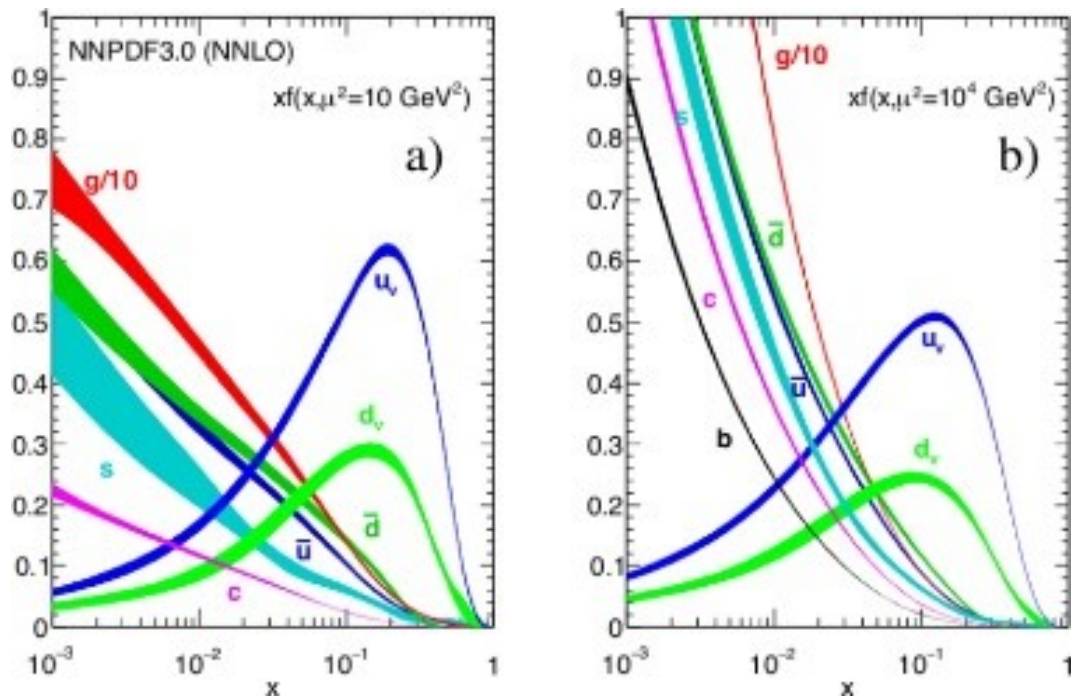


Figure 4-12: PDFs at two different Q^2 values

Chapter 5

Jefferson Lab and CLAS12 Experimental Setup

5.1 JLab 12 GeV CEBAF Machine

5.1.1 Injector

5.1.2 Accelerator and Beam Structure

What was the deal with looking into the time structure of the beam at JLab? Jan 2020 Is beam polarized?

5.1.3 Other notes and comparison to CERN

Chapter 6

Other Halls

6.1 Hall A

6.1.1 General Layout

6.1.2 Tritium Experiment Notes

6.1.3 BDX

6.1.4 DVCS and DVMP Notes

6.2 Hall C

6.2.1 Who Cares

6.3 Hall D

6.3.1 Overview



Hall D is located on the other side of the other 3 Halls at JLab and gets one extra Linac run, so is the only one able to receive the full 12 GeV beam. This hall actually uses a photon beam instead of an electron beam, as described below. The main experiments here are GlueX, PrimeX, Charged Pion Polarizability Experiment, etc.

6.3.2 Photon Beam Production and Structure

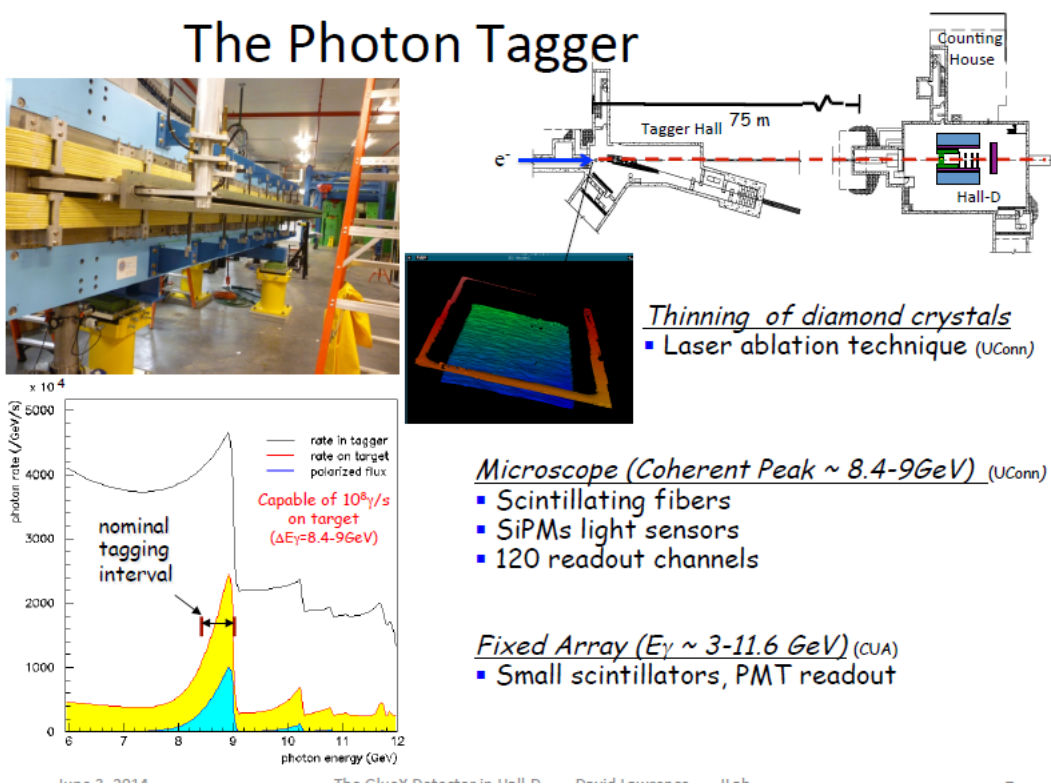


Figure 6-2: Hall D Coherent Brems. Photon Beam

glue x pair spectrometers

6.3.3 polarization measurement - triplet spectrometers?

6.3.4 GlueX Detector Specifications

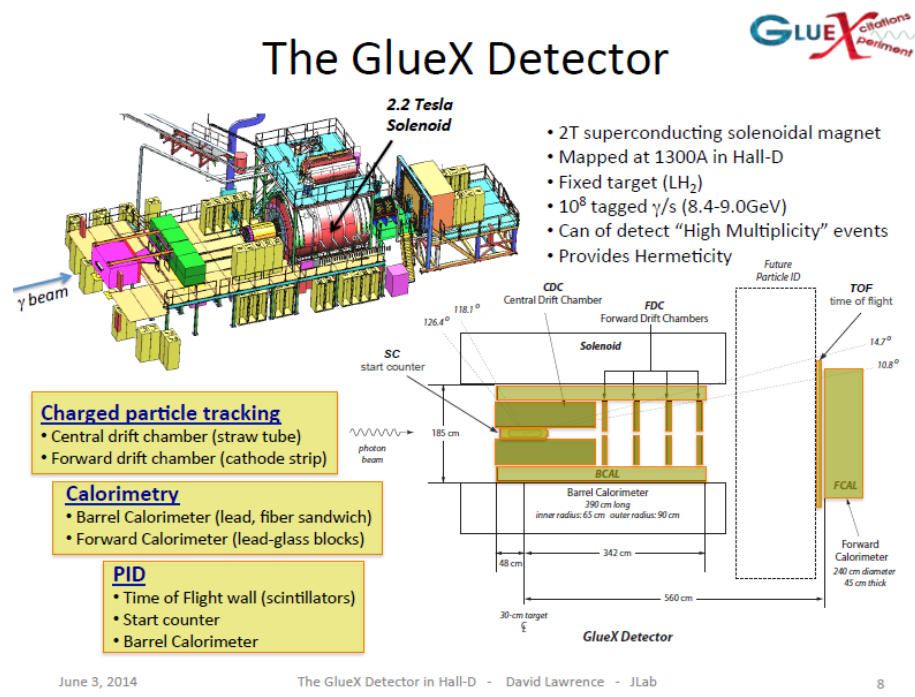


Figure 6-3: Hall D GlueX Detector

CDC - 60/40 Ar/CO₂ - 28 layers total - FADC 125 MHz - resolution - $\sigma_{r\phi} = 150 \mu\text{m}$

$\sigma_z = 1.5 \text{ mm}$

FDC - resolution $200 \mu\text{m}$

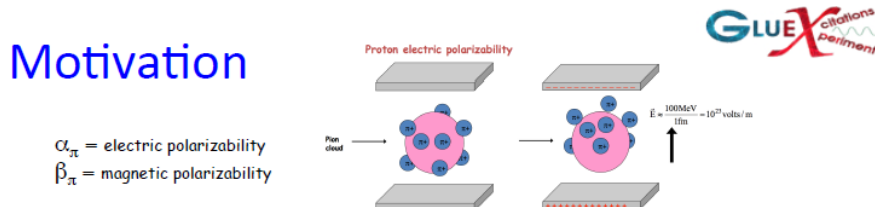
FCAL - 2800 lead glass blocks $4 \times 4 \times 45 \text{ cm}^3$ - PMT readout - resolution - $\frac{\sigma_E}{E} = \frac{5.7}{\sqrt{E}} + 2\%$

Hall D: Detector Design Parameters		
Capability	Quantity	Range
Charged particles	Coverage	$1^\circ < \theta < 160^\circ$
	Momentum Resolution (5° - 140°)	$\sigma_p/p = 1 - 3\%$
	Position resolution	$\sigma \sim 150$ - $200 \mu\text{m}$
	dE/dx measurements	$20 < \theta < 160^\circ$
	Time-of-flight measurements	$\sigma_{\text{ToF}} \sim 60 \text{ ps}; \sigma_{\text{BCal}} \sim 200 \text{ ps}$
	Barrel time resolution	$\sigma_\gamma \leq (74/\sqrt{E} \oplus 33) \text{ ps}$
Photon detection	Energy measurements	$2^\circ < \theta < 120^\circ$
	LGD energy resolution ($E > 60 \text{ MeV}$)	$\sigma_E/E = (5.7/\sqrt{E} \oplus 2.0)\%$
	Barrel energy resolution ($E > 60 \text{ MeV}$)	$\sigma_E/E = (5.54/\sqrt{E} \oplus 1.6)\%$
	LGD position resolution	$\sigma_{xy} \sim 0, 64 \text{ cm}/\sqrt{E}$
	Barrel position resolution	$\sigma_z \sim 0.5 \text{ cm}/\sqrt{E}$
DAQ/trigger	Level 1	$< 200 \text{ kHz}$
	Level 3 event rate to tape	$\sim 15 \text{ kHz}$
	Data rate	300 MB/s
Electronics	Fully pipelined	$250 / 125 \text{ MHz fADCs, TDCs}$
Photon Flux	Initial: 10^7 g/s	Final: 10^8 g/s

Figure 6-4: Hall D GlueX Detector Design Specifications

6.3.5 Example Experiment: Charge Pion Polarizability

Electric and Magnetic polarizabilities (α_π and β_π) are fundamental properties of particles with structure, such as the pion. In the low energy sector of QCD they can be related to the pion form factors F_A and F_V . Leading order calculations from ChPT calculate α_π and β_π to be equal in magnitude.



- α_π and β_π are related to the charged pion weak form factors F_V and F_A :
$$\alpha_\pi = -\beta_\pi = \frac{4\alpha_{EM}}{m_\pi F_\pi^2} (L_9^r + L_{10}^r) \propto \frac{F_A}{F_V}$$
where the low-energy constants L_{10}^r and L_9^r are part of the Gasser-Leutwyler effective Lagrangian
- Tests even-parity part of the Chiral Lagrangian
(odd-parity sector tested via anomalous processes such as $\pi^0 \rightarrow \gamma\gamma$)
- Reduce uncertainty of SM prediction of anomalous magnetic moment:
 $(g_\mu - 2)/2$ (see K. Engel, H. Patel, M. Ramsey-Musolf, arXiv:1201.0809v2 [hep-ph] and arXiv:1309.2225 [hep-ph])

Figure 6-5: Explanation for CPP Experiment

Experiments have been done to measure these quantities, but they do not agree with each other or ChPT:

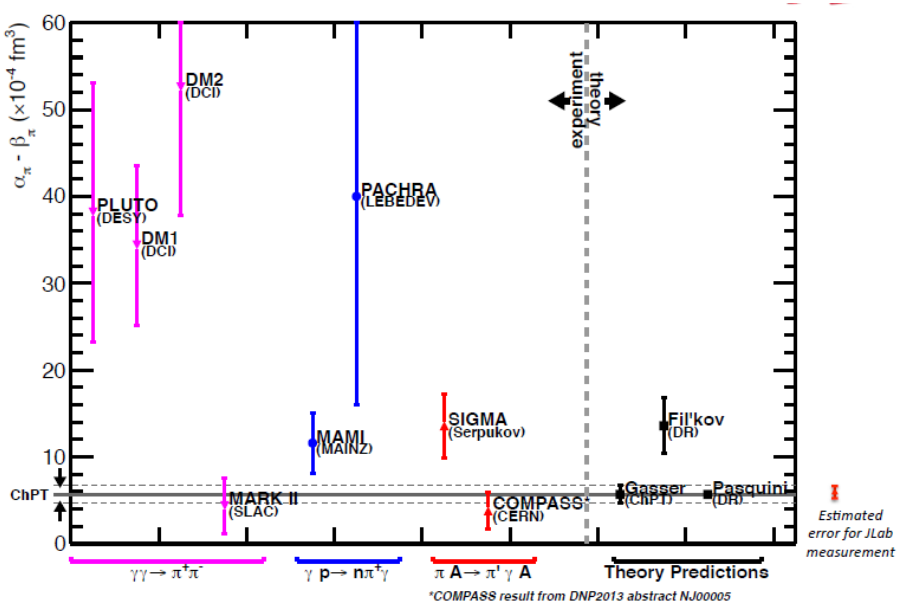
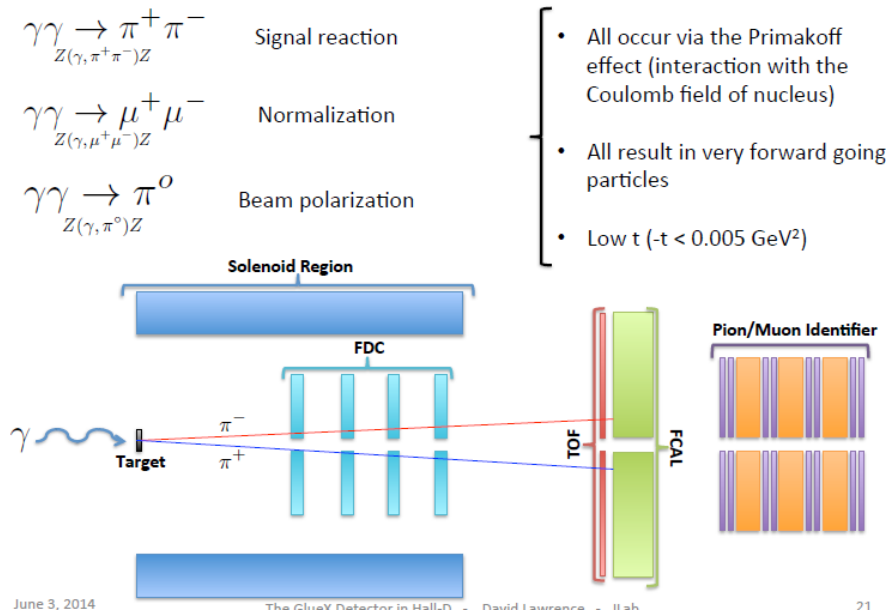


Figure 6-6: Phase Space Plot of CPP Experiments

Thus, the CPP experiment is proposed to run at glueX via the Primakoff effect ($\gamma\gamma \rightarrow \pi\pi$). The polarizabilities will be measured as the cross section depends on these values, a factor of two difference results in a $\sim 10\%$ difference in cross section.

Experimental Setup



June 3, 2014

The GlueX Detector in Hall D - David Lawrence - 18sh

21

Figure 6-7: Experimental Setup for CPP Measurement

[Detector specs here](#)

Chapter 7

CLAS12 System

7.1 Overview

7.1.1 Introduction

The CLAS12 detector is a large angle spectrometer that generally covers angles from 5 to 130 degrees, spanned by two main detector subsystems - the Forward Detector and the Central Detector.

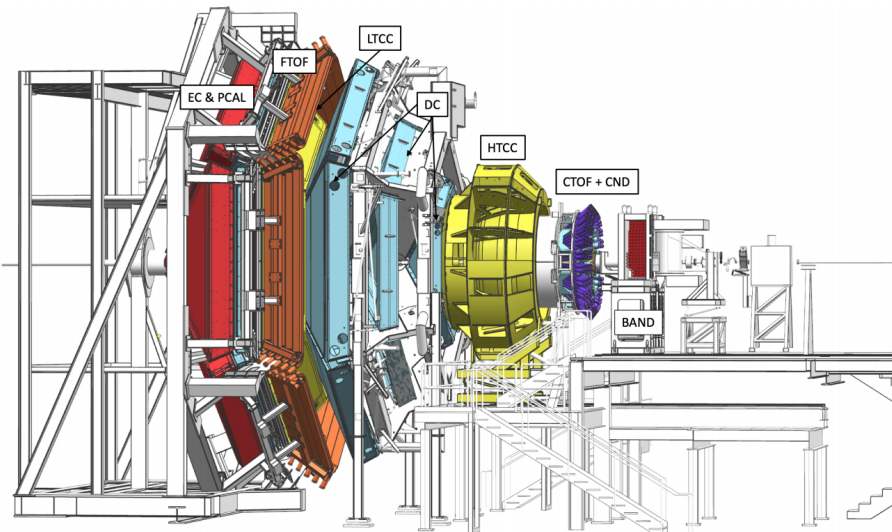


Figure 7-1: CLAS12 Detector System

Capability	Quantity	Status
Coverage & Efficiency	Tracks (FD)	$5^\circ < \theta < 35^\circ$
	Tracks (CD)	$35^\circ < \theta < 125^\circ$
	Momentum (FD & CD)	$p > 0.2 \text{ GeV}$
	Photon angle (FD)	$5^\circ < \theta < 35^\circ$
	Photon angle (FT)	$2.5^\circ < \theta < 4.5^\circ$
	Electron detection (HTCC)	$5^\circ < \theta < 35^\circ, 0^\circ < \phi < 360^\circ$
	Efficiency	$\eta > 99\%$
	Neutron detection (FD)	$5^\circ < \theta < 35^\circ$
	Efficiency	$\leq 75\%$
	Neutron detection (CD)	$35^\circ < \theta < 125^\circ$
	Efficiency	10%
Resolution	Neutron Detection (BAND)	$155^\circ < \theta < 175^\circ$
	Efficiency	35%
	Momentum (FD)	$\sigma_p/p = 0.5 - 1.5\%$
	Momentum (CD)	$\sigma_p/p < 5\%$
	Pol. angles (FD)	$\sigma_\theta = 1 - 2 \text{ mrad}$
	Pol. angles (CD)	$\sigma_\theta = 10 - 20 \text{ mrad}$
	Azim. angles (FD)	$\sigma_\phi < 1 \text{ mrad}/\sin \phi$
	Azim. angles (CD)	$\sigma_\phi < 1 \text{ mrad}$
	Timing (FD)	$\sigma_T = 60 - 110 \text{ ps}$
	Timing (CD)	$\sigma_T = 80 - 100 \text{ ps}$
Operation	Energy (σ_E/E) (FD)	$0.1/\sqrt{E} \text{ (GeV)}$
	Energy (σ_E/E) (FT)	$0.03/\sqrt{E} \text{ (GeV)}$
DAQ	Luminosity	$L = 10^{35} \text{ cm}^{-2}\text{s}^{-1}$
	Data Rate	20 kHz, 800 MB/s., L.T. 95%
	Solenoid	$B_0 = 5 \text{ T}$
Magnetic Field	Torus	$\int B dl = 0.5 - 2.7 \text{ Tm at } 5^\circ < \theta < 25^\circ$

Figure 7-2: CLAS12 Specification

GlueX Data Rates					
David Lawrence, Jefferson Lab					
	Front End DAQ Rate	Event Size	L1 Trigger Rate	Bandwidth to mass Storage	
JLab	GlueX	3 GB/s	15 kB	200 kHz	300 MB/s
JLab	CLAS12	0.1 GB/s	20 kB	10 kHz	100 MB/s
LHC	ALICE	500 GB/s	2,500 kB	200 kHz	200 MB/s
LHC	ATLAS	113 GB/s	1,500 kB	75 kHz	300 MB/s
LHC	CMS	200 GB/s	1,000 kB	100 kHz	100 MB/s
LHC	LHCb	40 GB/s	40 kB	1000 kHz	100 MB/s
BNL	STAR	50 GB/s	1,000 kB	0.6 kHz	450 MB/s
BNL	PHENIX	0.9 GB/s	~60 kB	~ 15 kHz	450 MB/s

* Jeff Landgraf Private Comm. 2/11/2010
** CHeP2006 talk Martin L. Purschke, current capability is 800MB/s peak, 500MB/s sustained (priv. comm. 2/14/2010)

June 3, 2014 The GlueX Detector in Hall-D David Lawrence JLab 31

Figure 7-3: CLAS12 Data Rates, Compared to Other Experiments

7.2 Target and Other

7.2.1 Beam from JLab

For entry into CLAS12, the beamline specs are as follows:

Beam current: up to 50 nA

Beam energy spread: 10^{-4}

Beam size: Less than 0.4 mm

Beam stability: Less than 0.1 mm

Beam halo: 10^{-4}

Beam polarization: up to 80%

7.2.2 Liquid Hydrogen Target

The hydrogen target in RGA is cooled to 20 K using a He4 evaporation fridge. Can be polarized by dynamic nuclear polarization, driven by a 140 GHz microwave source, can reach 90% polarization for protons, 40% for deuterons (both longitudinally polarized). The polarization can be measured by a Q-meter based NMR. 2.5 cm diameter target, extended 5 cm long.

RGA does not use a polarized target. The beam is polarized, but the target is not, so polarization is not helpful for extracting the 5-fold differential cross section (but it would be if the target was also polarized, and is useful for BSA measurements).

7.2.3 Luminosity Measurement

Luminosity in CLAS12 is measured from the Faraday Cup and using reference reactions such as elastic scattering. We don't use the Faraday Cup event by event, but we do use it run by run. For beam current measurements, beam position monitors upstream are used - but this is for monitoring on-line, not for analysis.

7.2.4 Moller Polarimeters

As stated, for RGA, the fact that the beam is polarized is not useful, but it is true and is measured by Moller Polarimeters.

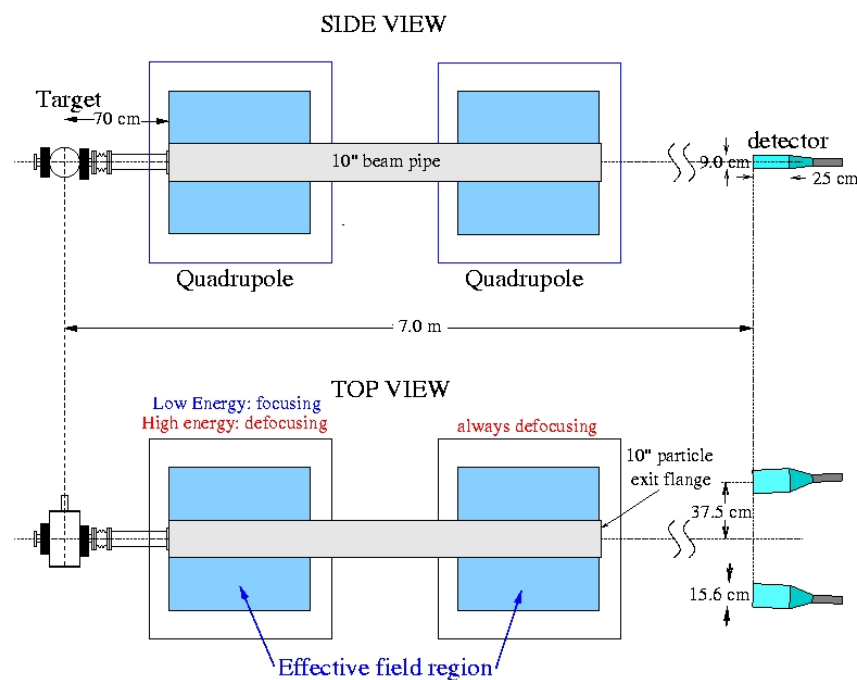


Figure 7-4:

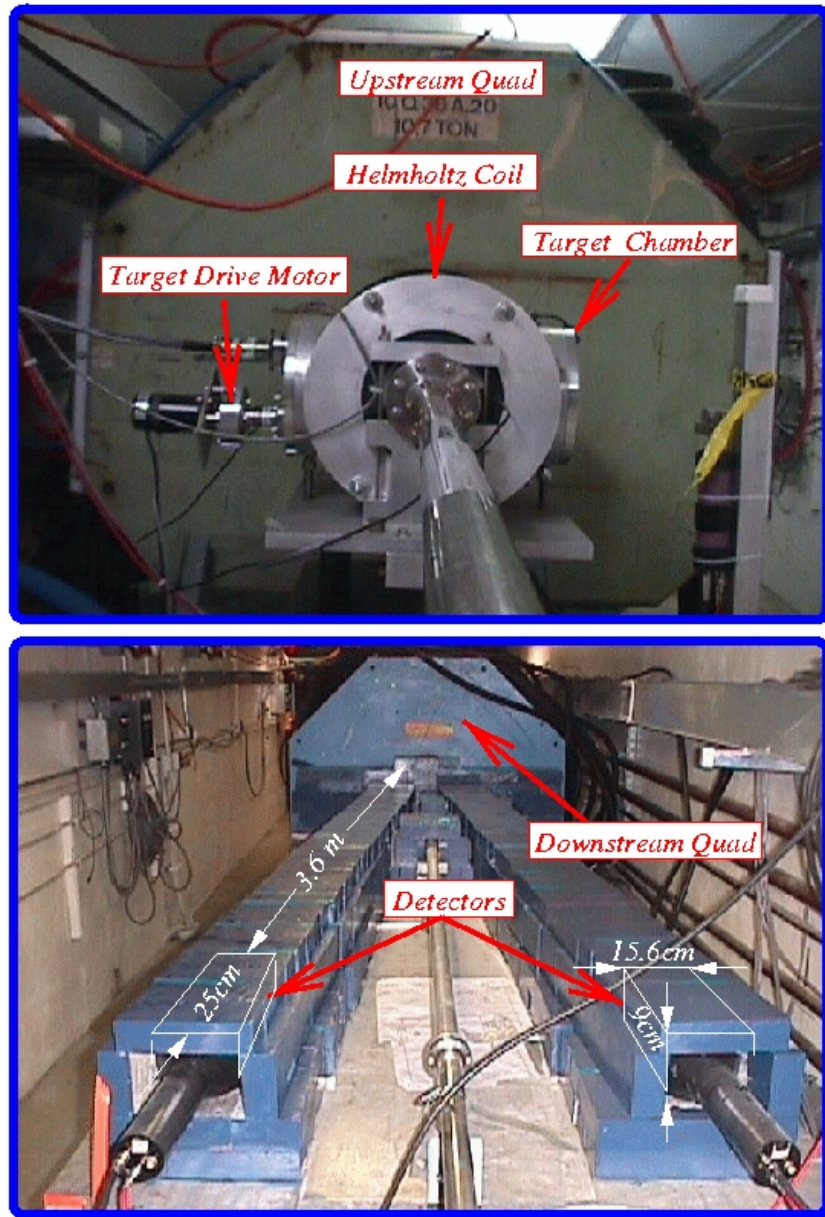
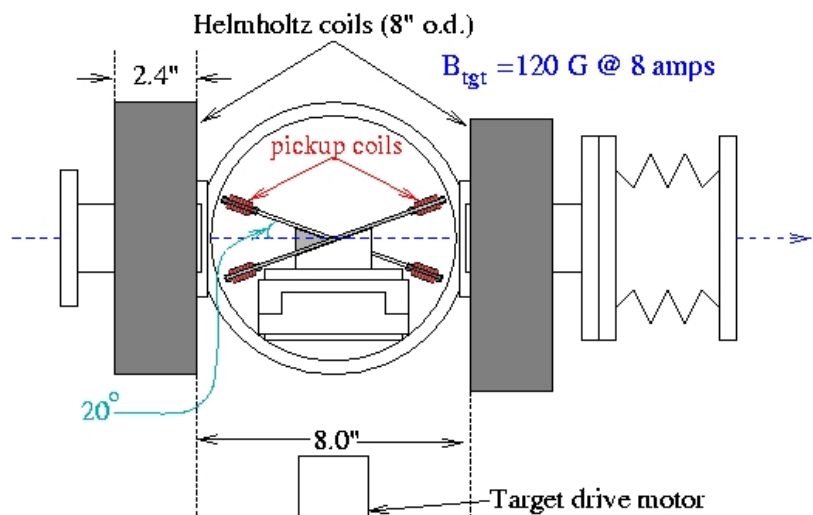


Figure 7-5:

Target Assembly

Side view



Top view

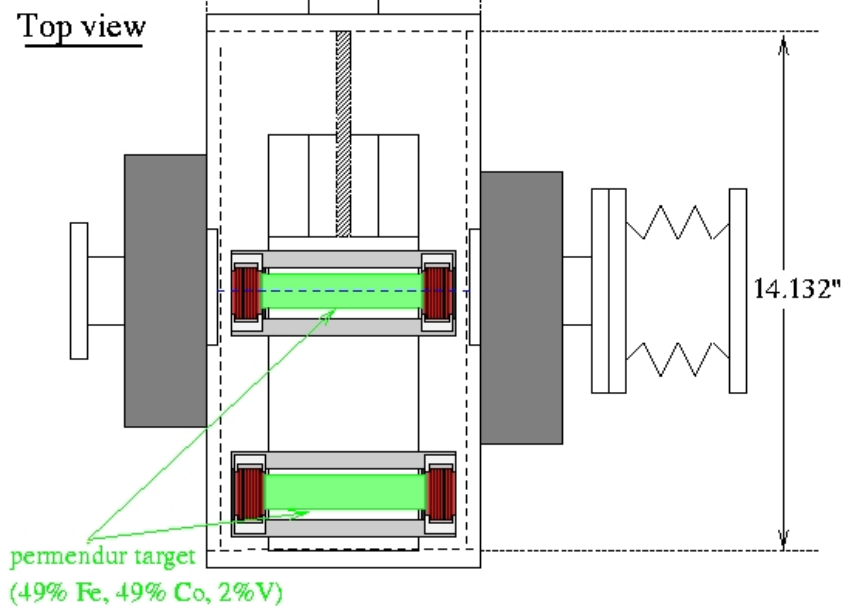


Figure 7-6:

7.2.5 Trigger

CLAS12 runs with "open trigger", which means different sub-experiments can define their own triggering logic. There is a standard electron trigger, based off of hits in HTCC, ECal, and FTOF.

7.2.6 Faraday Cup

Can manage 175 Watts - 17 nA at 10 GeV. Is used to calibrate beam current, needs a blocker in at higher currents.

7.3 Central Detector

Overview: The Central Detector spans roughly 35 to 125 degrees, and contains 4 sub-detectors, all in a 5 Tesla solenoidal field. The 5 detectors are: SVT, MMVT, CTOF, and CND.

7.3.1 SVT

The Silicon Vertex Tracker (SVT) covers from 35 to 125 degrees in θ . Has 8 layers (4 concentric rings) with 10, 14, 18, and 24 sectors respectively, double sided. 2π angular coverage. Read out with ASICs- FSSR2s. Designed to operate at 10^{35} luminosity, momentum resolution of $\sim 5\%$ for 1 GeV particles with $\theta = 90$ degrees. 42 cm long, 4 cm wide, 0.4 cm thick. Spatial resolution of $50 \mu\text{m}$, momentum resolution $\sim 5\%$, theta resolution 10 mrad, phi resolution 5 mrad. 33,792 total readout channels. Sensor thickness is $320 \mu\text{m}$, readout pitch $156 \mu\text{m}$. Supported by rohacell and carbon fiber backing to reduce material budget, at $\sim 1\%$ of a radiation length.

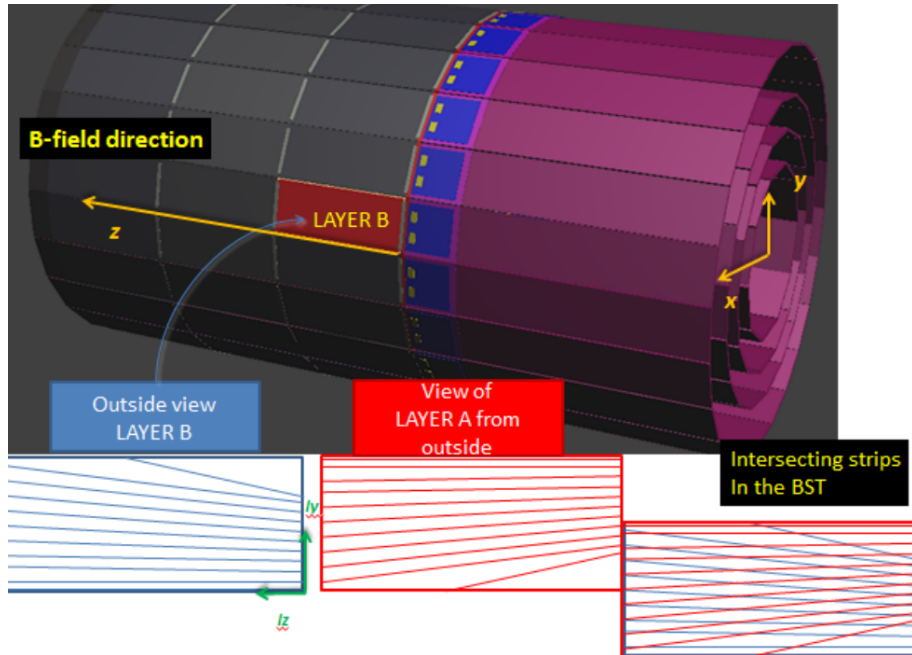


Figure 7-7: Silicon Vertex Tracker

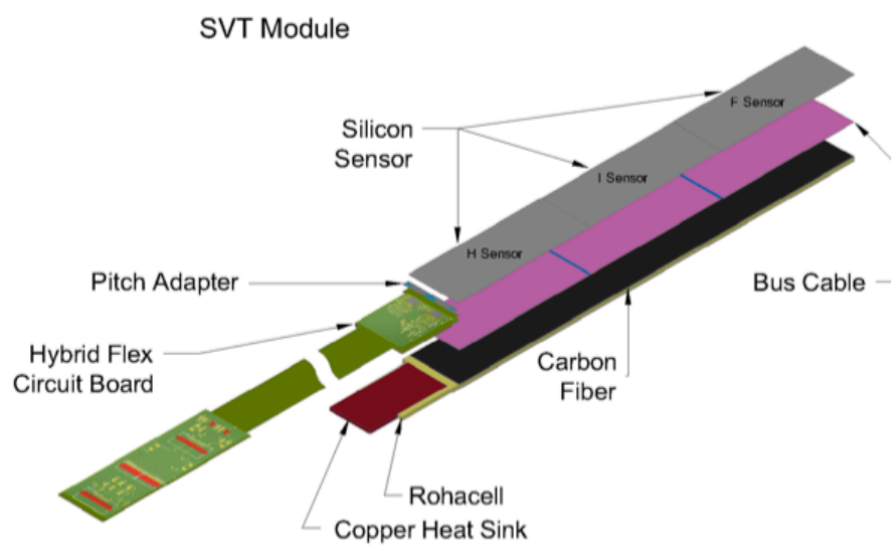


Figure 7-8: SVT Strip

7.3.2 MMVT

Composed of two parts: a **Barrel Tracker** and a **Forward Tracker**. PCB is 200 μm thick, 0.3% of a radiation length. 20 MHz sampling frequency. Time resolution

of 10 ns. 500 μm strip pitch.

Advantages of MMVT for CLAS12 :

Price: much cheaper compared to SVT. For large area, the price become rapidly prohibitive. Material: Since it is a gasesous detector, it is good for the material budget. Physics Requirements: Not as good spatial resolution as SVT, but can resolve polar angle better. Optimal performance is actually achieved with a combination of both detectors are used.

Overall momentum uncertainty (σ_p/p) = 1.6%. $\sigma_\theta = 1.4$ mrad. $\sigma_\phi = 2.6$ mrad. $\sigma_z = 270$ mm.

Barrel Tracker

18 cylindrical detectors arranged in 6 layers. Covers 35 to 125 degrees. 15,000 readout elements. Gas Mixture 90% Argon, 10% isobutane. 3 mm drift gap. 5 kV/cm field. 75% mesh transparency.

Forward Tracker

6 circular, flat detectors from 6 to 29 degrees in θ . Improves vertex resolution by a factor of up to 10x compared to just the drift chambers along. 6,000 readout elements. 80% neon, 10% ethane, 10% Carbon Tetrafluoride. 5 mm drift gap. 1kV/cm field. 100% mesh transparency.

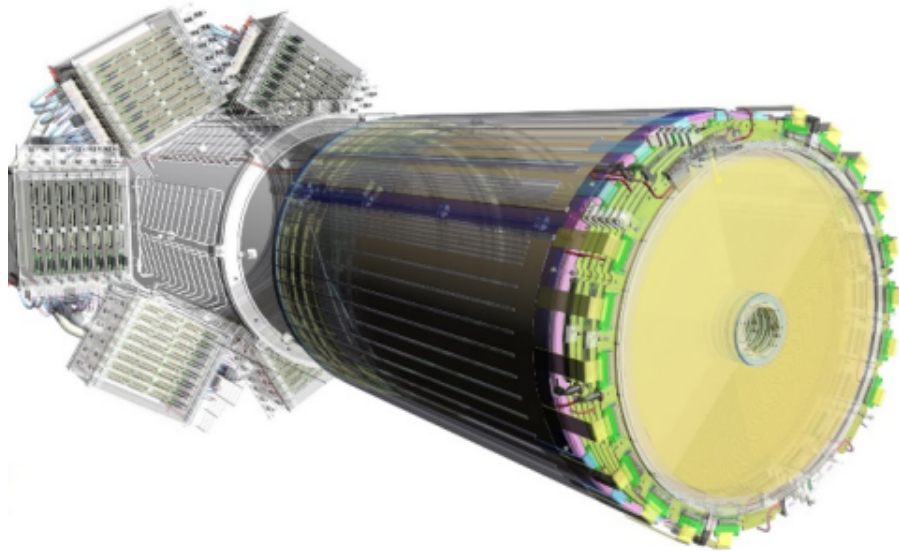


Figure 7-9: SVT Strip

7.3.3 CTOF

Central for PID purposes. Divides into 48 1 meter long plastic scintillators with double sided PMT readout. PMTs are in the 0.1 T fringe field region and enclosed in magnetic shielding. 65 picosecond timing resolution. 35 to 125 degrees, 2π in polar angle. 3 cm x 3 cm scintillator planks. Pion/Kaon separation up to 0.64 GeV, Kaon/proton separation up to 1 GeV, pion proton separation up to 1.25 GeV.

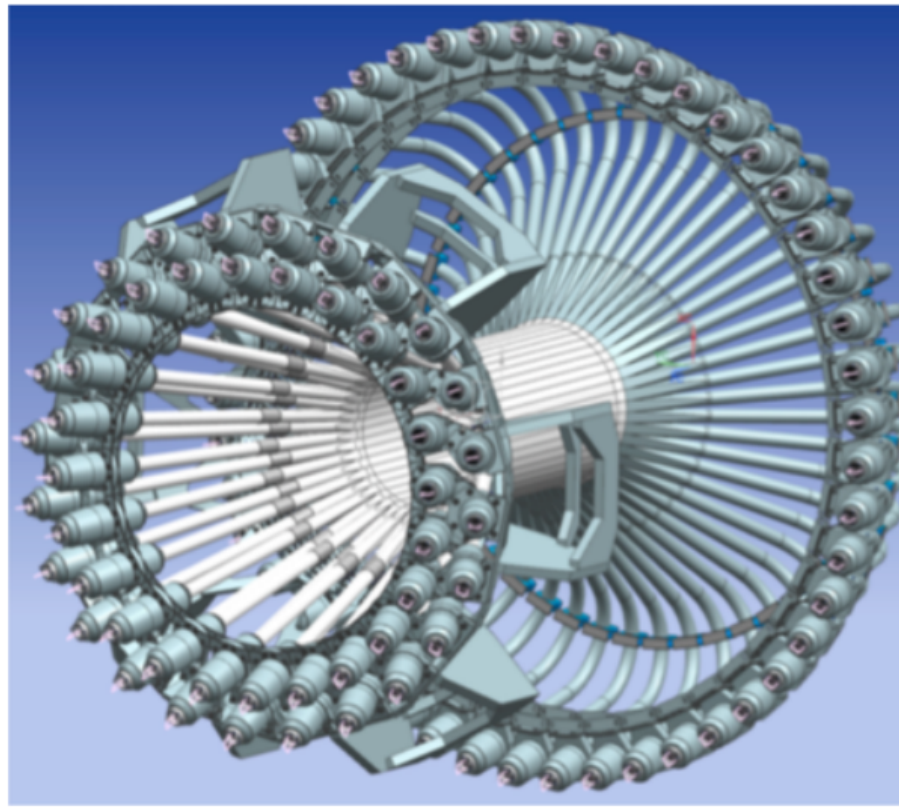


Figure 7-10: SVT Strip

7.3.4 CND

Detects 0.2-1 GeV neutrons. 3 layers, 48 paddles per layer. Plastic scintillator, 3 cm x 3cm, 0.7 meters long. Neutron detection efficiency $\sim 10\%$. 130 picosecond timing resolution, 2 degrees angular resolution (polar and azimuth).

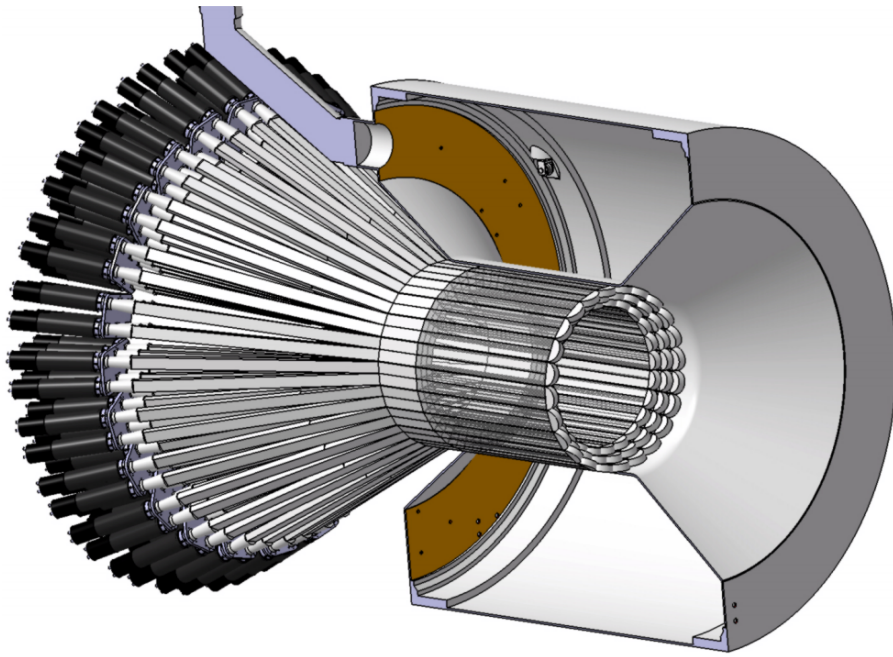


Figure 7-11: SVT Strip

7.3.5 Solenoid

5 Tesla super conducting magnet, uniform field ($\Delta B/B = 10^{-4}$). Weakest at small angles, strongest at large angles. Opening polar angle of 40 degrees. Momentum range of interest 0.3 to 1.3 GeV. 18 Megajoules stored energy. 85 cm in diameter, 4.2 Kelvin operation.

7.4 Forward Detector

Overview:

7.4.1 HTCC

Used basically as an electron trigger. Composed of 60 lightweight ellipsoidal mirrors, that focus Cherenkov light onto eight 5-inch phototubes (48 channels on entire HTCC). Working gas is CO₂ at STP ($n=1.0005$, $\theta_{max} = 1.7$ degrees, covers 5 to 35 degrees, 2π in azimuth. Active area 2.4 meters in diameter. Electron signal threshold is 15 MeV,

charged pion threshold is 5 GeV. 99.9% electron detection efficiency vs. pions. 15 feet in diameter, 6 feet long. Mirror thickness is 0.1 g/cm^2 . Kaons have no signal, as they would need 16 GeV to generate a signal. Uses Winston cones to increase collection efficiency. 20 photoelectrons per electron in HTCC, 25% quantum efficiency. The PMTs have 14 dynodes, gain of about 10^7 . HTCC material budget 0.135 g/cm^2

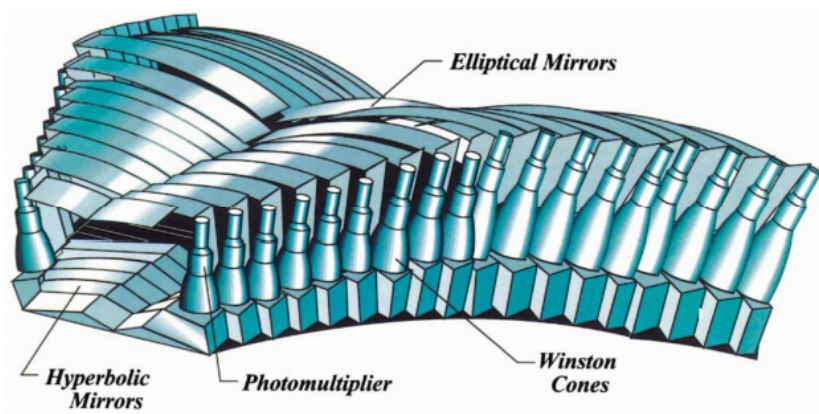


Figure 16: Layout and components of the optical mirror system within each LTCC box from the design model.

Figure 7-12: SVT Strip

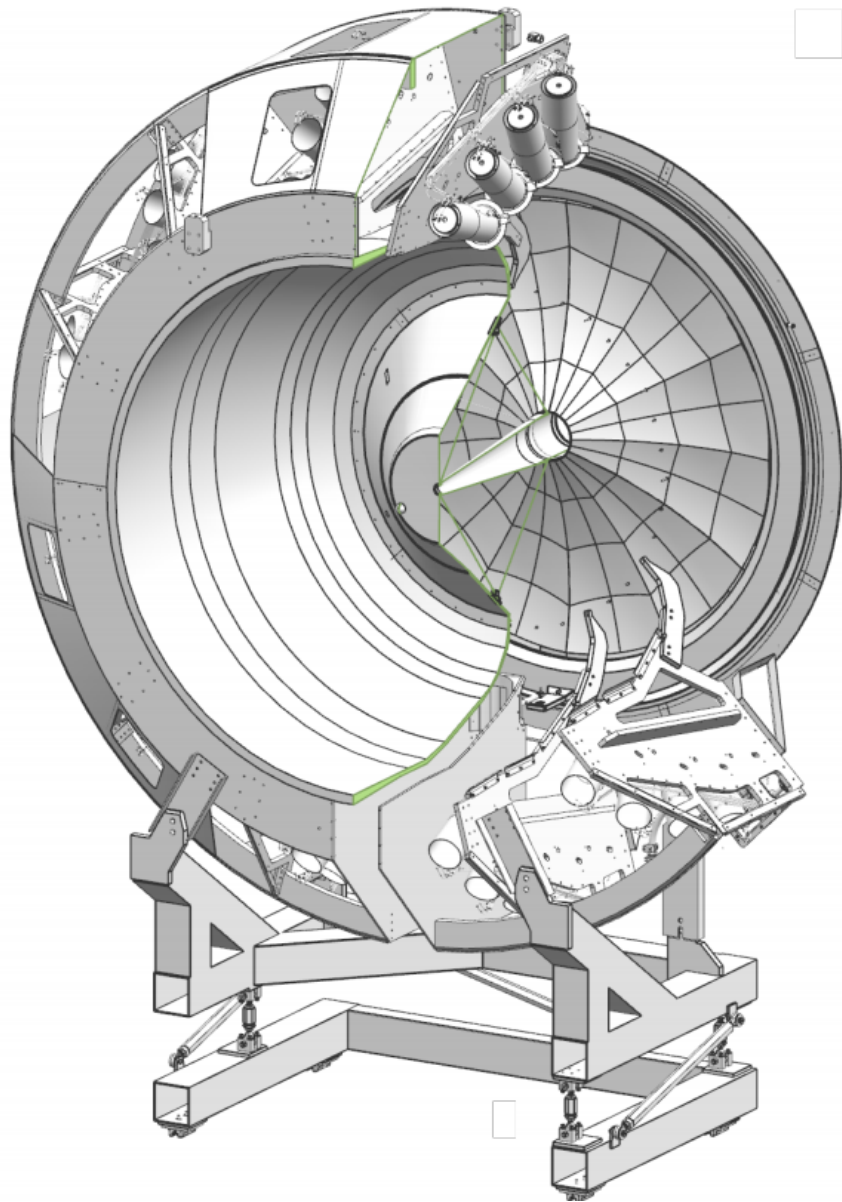


Figure 7-13: SVT Strip

7.4.2 Torus

6 coil torus, 4k amps, 3.5 Tesla torodial field, supercritical LHe cooled. 14.2 Megajoules stored energy. 2 Henries of inductance. Field strongest at small angles, weakest at large angles. Inbending vs out bending: I have been wondering about this as well. All I know is that inbending and outbending have different acceptances. So, I guess some channels prefers inbending while the others do outbending? I'm not sure though.

FX claims outbending results have better quality for these days.

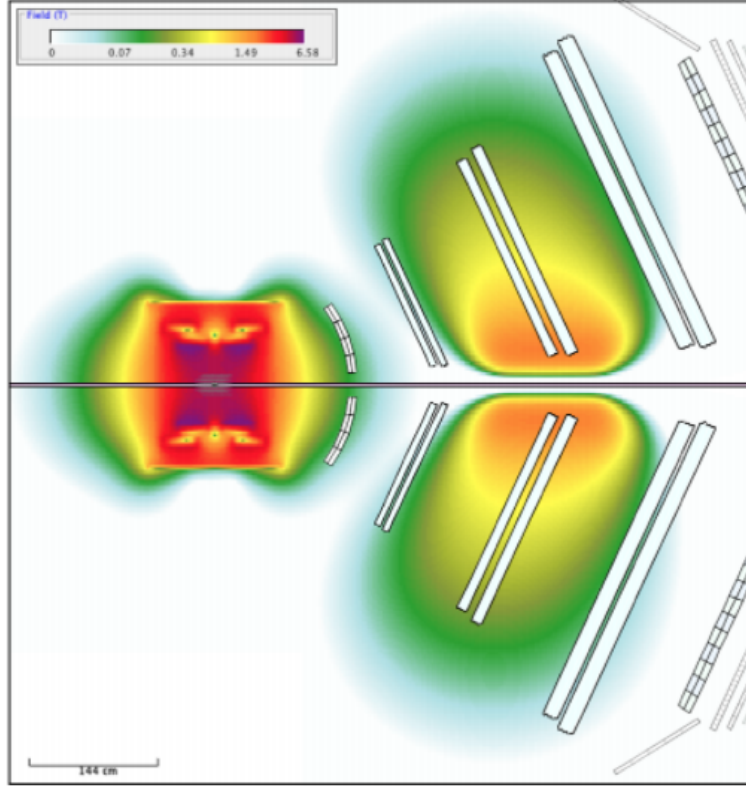


Figure 6: Combined solenoid and torus magnetic fields. The color code shows the total magnetic field of both the solenoid and torus at full current. The open boxes indicate the locations and dimensions of the active detector elements.

Figure 7-14: SVT Strip

7.4.3 Drift Chambers

There are 3 layers of drift chambers, each with 6 sections. Each chamber has 2 superlayers of 6 layers by 112 wires, for a total of 24,192 wires. (Structure is 112 wires * 6 layers * 2 superlayers * 18 DC sections = 24,192 wires). Physical wire sectioning looks like:

(IIIIII)-(IIIIII)—(IIIIII)-(IIIIII)—(IIIIII)-(IIIIII) x 6 sectors

Where each "I" is a layer of 112 wires.

Spatial resolution is $300 \mu\text{m}$, angular coverage 5-40 degrees. Momentum resolution

$\Delta p/p < 1\%$, angular resolution is 1 mrad in theta, $1\text{mrad}/\sin \theta$ for phi. The Drift Chambers are located 2, 3, and 4 meters from the gas mixture is 90/10 Argon/CO₂. Time resolution = ?

DC specifics: 30 micron diameter tungsten sense wires, 80 micron Cu-Be field wires, 140 micron Cu-Be guard wires. 20 g tension on sense, 62 g tension of field, 180 g on guard. Max sag calculated to be on order of 10 microns.

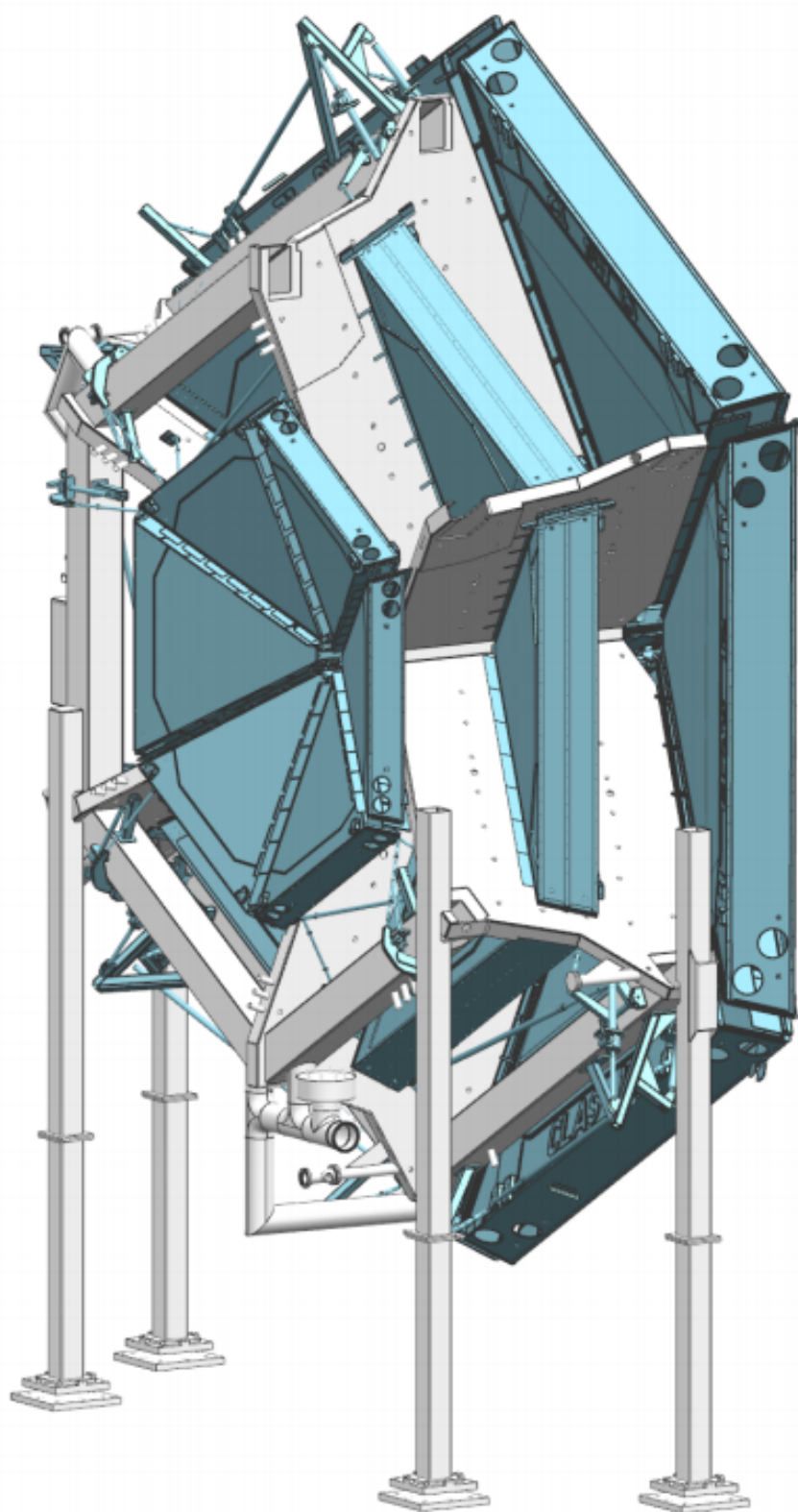


Figure 7-15: SVT Strip

7.4.4 LTCC

6 sectors, perfluorobutane (C_4F_{10}) $\rightarrow n = 1.0013 \rightarrow \theta_{max} = 3$ degrees. Electron threshold 9 MeV, pion threshold 2.7 GeV, Kaon threshold 9.4 GeV. Allows for good pion/kaon discrimination from 3.5 GeV to 9 GeV.

Each section has 108 mirrors, 36 winston cones, and 36 PMTs. Mirror is aluminium with MgF_2 coating. Kevlar support structure. Perflourobutane is 100% transparent above 220 nm light.



Figure 7-16: Low Threshold Cherenkov Counter

7.4.5 RICH

Provides PID in the range of 3-8 GeV, replacing one sector of LTCC (right middle sector). Pion/Kaon rejection factor > 500 , Kaon/Proton rejection factor > 100 . Covers 5 to 25 degrees in theta, uses aerogel ($n=1.05 \rightarrow \theta_{max} = 18$ degrees). Pion threshold 460 MeV, Kaon threshold 1.6 GeV. Read out by 64 channel photomultipliers.

$$\beta_{min}=0.95, \gamma_{min} = 3.3$$

What is angular resolution?

Reminder of relevant equation:

$$\cos \theta = \frac{1}{\beta n} \longrightarrow \theta = \arccos \frac{1}{\beta n} \quad (7.1)$$

$$\gamma = \frac{1}{\sqrt{1 - \beta^2}} \longrightarrow \beta = 1 - \frac{1}{1 - \gamma^2} \quad (7.2)$$

	momentum	$\sim \gamma$	θ
pion	3	21	17.4
kaon	3	6	12
pion	5	36	17.6
kaon	5	10.1	15.9
pion	8	57.1	17.7
kaon	8	16	17.1

Detector	Scintillator	PMT
FTOF - 1a	BC-408	Phillips XP2262, EMI 9954A
FTOF - 1b	BC-404	Hama. R9779
FTOF - 2	BC-408	EMI 4312KB
PCAL	FNAL	Hama. R6095
ECAL	BC-412	Philips XP2262, EMI 9954
CND	EJ-200	Hama. R10533
CTOF	BC-408	Hama. R2083
HTCC	N/A	ET 9823QKB
LTCC	N/A	200 Photonis XP 4500B
LTCC	N/A	16 Photonis XP 4508 (Quartz Window)

*ET stands for Electron Tube, a company. Could not find a spec sheet for this

PMT type. ** Could not find spec sheets for either HTCC, or LTCC PMTs.

Scintillator	Detectors	Principal Use/Features	L.O.	WME	R/D Time	L.A.	Length
BC-404	FTOF-1b	Fast Counting	68	408	0.7/1.8	140	
BC-408	FTOF-1b,2,CTOF	TOF - Large Area	64	425	0.9/2.1	210	
BC-412	ECAL	Large Area	60	434	1.0/3/3	210	
EJ-200	CND	Long attenuation, fast	64	425	0.9/2.1	380	

L.O - Light Output - % Anthracene WME - Wavelength Maximum of Emitted Photons R/D Time - Rise / Decay time (ns) L.A. Length - light attenuation length (cm)

All scintillators have a PVT (Polyvinyltoluene) base.

EJ-200: 200 – 10K photons per 1 MeV.

Thermal effects: EJ-200 loses 5% of its light output between 20 degrees C and 60 degrees C. No change between -60 to 20 degrees C.

PMT	Det.	TS/A	WVE	PHTC	DNY	Anode	Time Resp.
Hama. R6095	PCAL	28/25	300/420/650	BA/BSG	B&L/11/2.1	1500/0.1	4/30/3
Hama. R9779	FTOF-1b	51/46	300/420/650	BA/BSG	LF/8/0.5	1750 /0.1	1.8/20/0.25
Hama. R10533	CND	51/46	300/420/650	BA/BSG	LF/10/4.2	1000/0.1	2/24
Hama. R2083	CTOF	51/46	300/420/650	BA BSG	LF/8/2.5	3000/0.2	0.7/16/
Phillips XP2262	FT1a ECAL						
EMI 9954A	FT1a ECAL						
EMI 4312KB	FTOF-2						

No spec sheets could be found for the PMTs used in the TFOT1a, ECAL, or FTOF-2. Typical dark currents for all PMTs are 100 nA.

Tube size / photocathode area (diameter in mm) Wavelength short / peak / long (nm) Photocathode / window material (BA = Bialkali, BSG = Borosilicate Glass) Dynode structure / stages / gain LF = Linear-focused, B&L = Box and line / / Gain - Gain x 10⁶ Anode to Cathode Voltage / Anode Current - Volts / mA Rise / transit time/time spread in ns

R10533 PMT R2083 PMT R9779 PMT R6095 PMT

CND Scintillator

BC Scint Specs from Saint Gobain

CND PMT

[CTOF PMT Spec sheet](#) Bialkali photocathode, 8 dynodes, 2.5×10^6 typical gain
Linear-focused dynode structure Window material Borosilicate glass peak wavelength
420 nm, range from 300 to 650 nm. Max anode to cathode voltage of 3500 V, made
anode current of 0.2 mA. Dark current around 100 nA.

7.4.6 FTOF

Used for PID, three layer system - 1a, 1b, and 2. Has a design resolution of 60 ps to 160 ps. Average scintillation rate 250 kHz. Pion/Kaon separation up to 2.8 GeV, Kaon Proton separation up to 4.8 GeV, pion proton separation up to 5.4 GeV.

6 meters away from target. Time resolution of 80 ps less than 36 degrees, 150 ps greater than 36 degrees. PMTs are shielded from CLAS12 torus. 6 sectors, plastic scintillator, double sided PMT readout. 3 panels - 1a - 23 counters, 1b - 62 counters, 2 - 5 counters.

15cm wide x 5 cm deep x 33 cm up to 376 cm long.

20-30 cm up to 15x5 130 ps

350-400 cm 6x6 60 ps

370 to 430 cm, 22x5cm, 150 ps

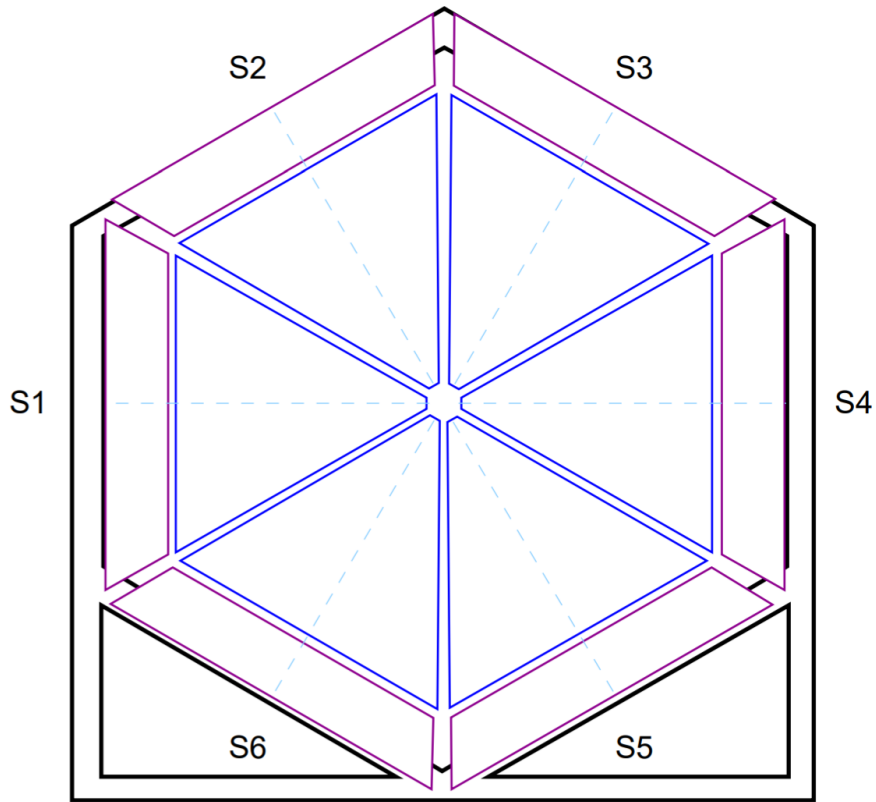


Figure 7-17: SVT Strip

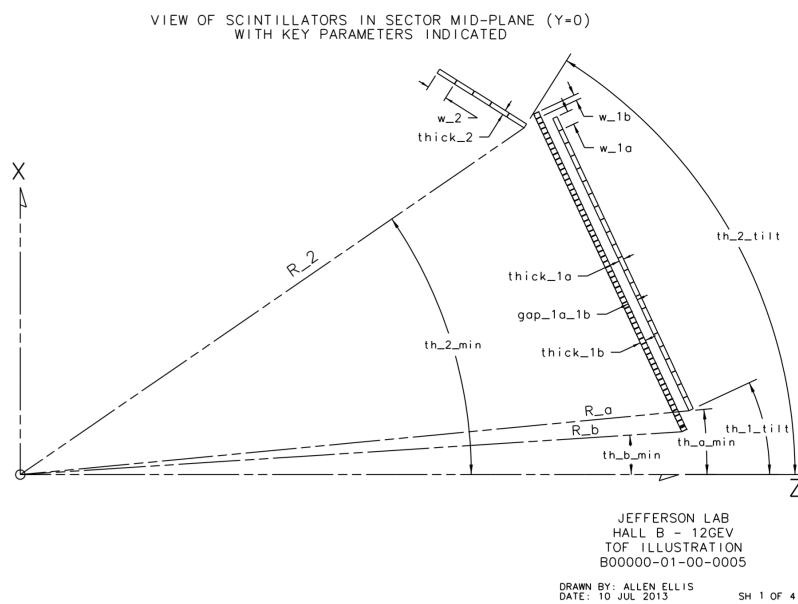


Figure 7-18: SVT Strip

The timing resolution minimums are for being close to the beam axis where particles are moving faster, and farther out from the beamline (larger theta) particles are moving slower so a less resolved time difference is acceptable.

1a

Coverage is 50% at 5 degrees to 85% at 35 degrees

Dimensions: L 32.3 cm to 376.1 cm, wxh = 15x5 cm

Material BC-408

PMTS: EMI 9954A, Phillips XP2262

Time resolution 90 - 160 ps small bar to big bars

1b

Coverage is 50% at 5 degrees to 85% at 35 degrees

Dimensions: L 17.3 cm to 407.9 cm, wxh = 6x6 cm

Material BC-404 (first half) and BC-408

PMTS: Hamamatsu R9779

Time resolution 60-110 ps small bar to big bars

2

Coverage is 85% at 35 degrees to 90% at 45 degrees

Dimensions: L 371.3 cm to 426.2 cm, wxh = 22x5 cm

Material BC-408

PMTS: EEMI 4312KB

Time resolution 140 - 165 ps small bar to big bars

For more FTOF specifications, look [here](#)

FTOF two panels: Official answer from CLAS12 FTOF NIM paper: "For tracks that pass through both arrays the combined time information (described in Ref. [10])

is used and results in a 20

I guess this is the right answer though: 1a is recycled one from CLAS while 1b is new one.

7.4.7 PCal and ECal

ECal from CLAs could only contain showers with $E < 5$ GeV. Above 5.5 GeV, couldn't resolve neutral pion gamma gamma angle, so needed PCAL. PCAL is 7 meters from target, ECAL is 7.5 M from target. EC segmentation 10 cm, PCAL finer segmentation. PCal 5.5 radiation lengths. 20.5 radiation lengths total. Both are sampling calorimeters, with PB and scintillator layers. The CLAS ECAL was resused and a new PCAL was installed in front of it. Primarily used for identification of electrons, photons, gamma gamma decays from pions, and neutrons. They are sampling calorimeters with six moduels. Each module has a triangular shape with 54 (15/15/24 - PCAL/ECALinner/ECALouter) layers of 1 cm htick scintillators segmented into 4.5/10 cm (PCAL/ECAL) wide strips and sandwiched between 2.2 mm thick lead sheets. The total thickness is about 20.5 radiation lengths.

Scintillator layers are grouped into three readout views with 5/5/8 PCAL/ECinner/ECouter, layers per view providing several cm resolution of energy clusters. Light from each scintillator readout group is routed to PMTs via flexible optical fibers.

Overall perfomance:

Energy resolution of 10%, position resolution of 2 cm, time resolution of 500 ps.

Are these the real statistics? Because they seem like BS.

BC-408

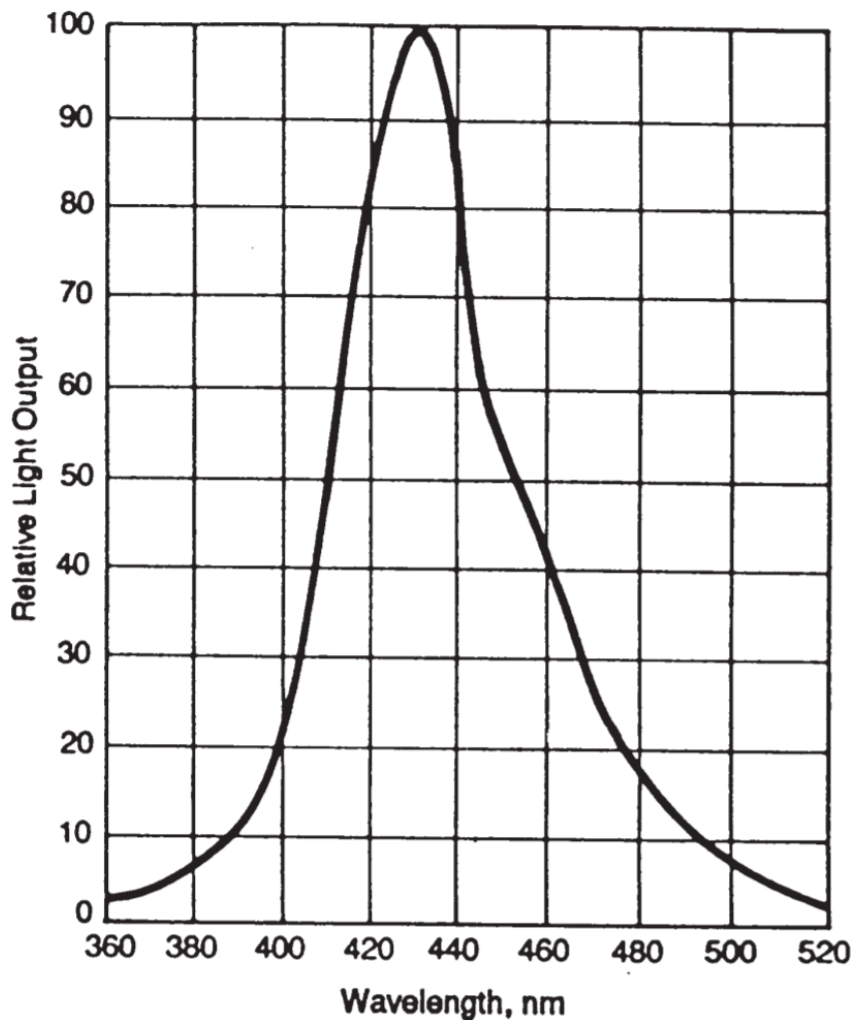


Figure 7-19: BC 408 Emission Spectra

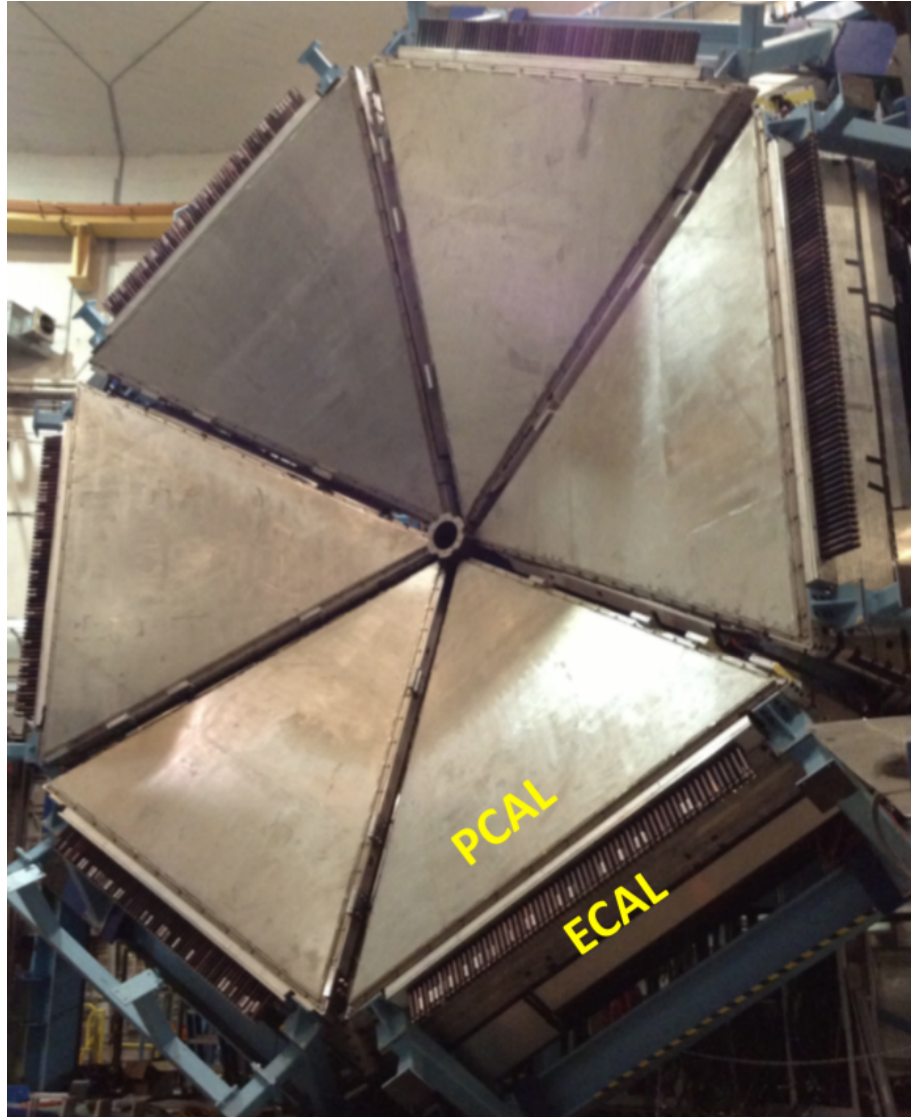


Figure 7-20: SVT Strip

PCAL

50% coverage at 5 degrees, 85% coverage at 35 degrees. 15 scintillators, 14 lead layers, per module. 1200 scintillator strips, $1 \times 4.5 \text{ cm}^2$ up to 432 cm long, with two holes along the strip, and 0.25 mm TiO₂ coating (reflective coating)

Lead sheets are 2.2 mm thick. Readout by fibers into 1 inch PMTs, Hamamatsu R6095. Light yield is 11-12 photo-electrons per MeV.

PCAL scintillator was manufactured at the FNAL-NICADD Extrusion Line Facil-

ity. Polystyrene base was Dow STYRON 663 W, primary dopant is 2,5 -diphenyloxazole (PPO, 1% by weight) - this is the organic scintillator, peaks at 385 nm:

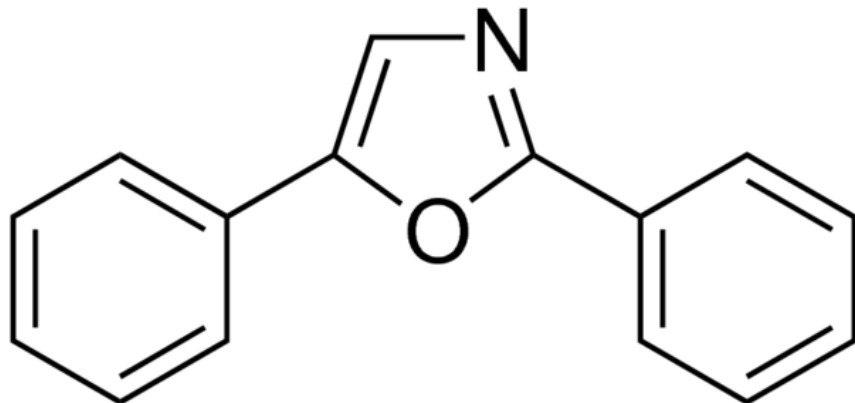


Figure 7-21: 2,5-diphenyloxazole

The Secondary dopant is 1,4 bis (5-phenyloxazol- 2-yl) benzene (POPOP, 0.03% by weight) - also scintillator, peaks at 410 nm.

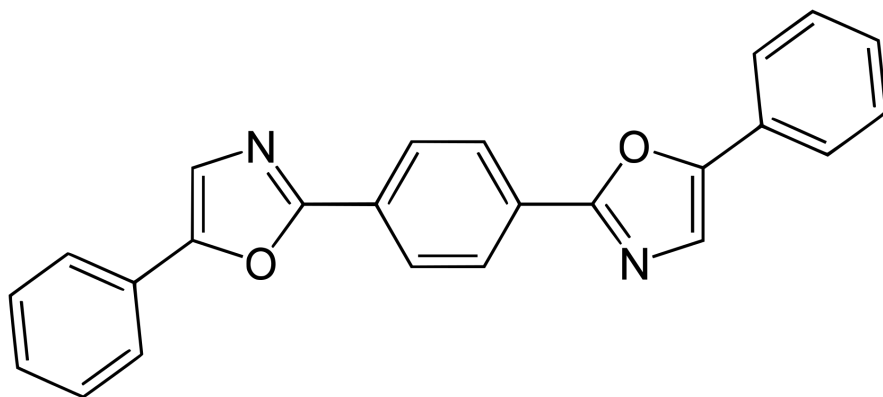


Figure 7-22: 1,4 bis (5-phenyloxazol- 2-yl) benzene

A reflective surface coating of polystyrene with 12% TiO₂ with 0.25 mm nominal thickness was co-extruded.

Cast plastic scintillator costs about \$50 per kg, while extruded scintillator is significantly lower in price - about \$10 per kg.

[Interesting write up on FNAL Scintillator extrusion](#)

[PCal Technical Report ECal Technical Report](#)

ECAL

50% coverage at 5 degrees, 85% coverage at 35 degrees. 39/38 scintillators / lead layers per module. 216 readout channels per module, 1200 strips per module. Strips are 1x10 to 12 cm² by up to 441 cm long, BC-412 (plastic scintillator with high light output, longest light attenuation length, [cheap!](#)). Lead sheets are 2.4 mm thick. Read out by fiber into 2 inch PMTs, Phillips XP2262 and EMI 9954. 3-4 photoelectrons/MeV deposited energy.

Other: Forward Tagger, BAND, not important.

20 kHz Level 1 trigger rate, 1 GB/s.

Only about 50% of the electron triggers recorded with an inbending torus polarity are actually electrons. For outbending torus polarity, hte electron trigger purity is as high at 70%.

[Detector Specs](#)

Outbending allows for lower Q2 measurements, inbending allows for slightly higher Q2 measurements.

By measuring DVMP, we can get information about GPDs in the following way – in the leading twist approximation / some other formalism bullshit, dvmp cross section is described by the generalized Compton form factors, which themselves are (to leading twist etc.) convolutions of GPDs, so the dvmp cross section sets constraints on GPD behavior.

hard exclusive pseudoscalar meson electroproduction in recent years has shown that the asymptotic leading twist approximation is not readily applicable in the range of kinematics accessible to current experiments. In fact, there are strong contributions from transversely polarized virtual photons that are asymptotically suppressed by $1/\alpha^w$ in the cross sections and have to be considered by introducing chiral-odd GPDs into the framework.

Hi Bobby, so sorry for late reply I was busy with readiness review preparation. So $Q_2 > 1$ is indeed for deeply virtual events, however it has no relation with lepton/hadron angle. There are pi0 events in the region below 1GeV², and they are

also pi0 events. The limit on 1GeV2 is somewhat artificial. Ideally we are looking at the asymptotic freedom, so Q2 should be infinity, but we are hoping that 1GeV2 is big enough to apply models that are based on asymptotic freedom. There are many terms also that are proportional to powers of t/Q^2 . So we need reasonably big Q2 to apply GPDs models. And in fact CLAS kinematics is often questioned to be too small for GPDs theoretical models.

Chapter 8

DVEP and GPDs - what are we here for

DVMP:

Deep exclusive processes can allow access to Generalized Parton Distributions (GPDs), a concept that lies at the root of 3D imaging of the proton's quark-gluon substructure, as GPDs contain information about the transverse spatial distribution of quarks and their longitudinal momentum inside hadrons. The key to extracting GPDs from experiments are the Quantum Chromodynamics (QCD) factorization theorems. Deeply Virtual Compton Scattering (DVCS) is the cleanest way to

study GPDs. While DVCS data have given hints of the factorization regime being attained, such hints have not been observed for Deeply Virtual Meson Production (DVMP) data. Exclusive π^0 electroproduction has been measured by experiment E12-06-114 in Hall A of JLab in order to test factorization in DVMP processes. Cross sections have been measured at three fixed Bjorken- x (x_B) : 0.36, 0.48 and 0.6 in the Q2 range 3 to 9 GeV². High statistical measurements of polarized and unpolarized cross sections of $H(e,e',\text{gamms}) p$ could allow mapping and extraction of GPD information from the nucleon. In this talk, I will show the experimental setup, calibration and preliminary results of the neutral pion electroproduction cross sections for $x_B > 0.3$ from this experiment.

8.1 GPDs

8.1.1 PDFs

8.1.2 The GTMD Cube

8.1.3 GPDs and Helicity Odd Structure Functions

8.2 DVEP

8.2.1 DVEP, DVCS, and DVMP

DVEP

DVCS

DVMP

8.2.2 How DVPiP Relates to GPDs

8.2.3 CLAS12 - DVMP Questions

Intuition about DVMP

First, note that not all DVMP reactions are sensitive to nuclear transversity distributions, which involves quark helicity flip of transversely polarized quarks helicity. This can occur in production of pseudoscalar mesons, e.g. pi0 and eta production, with spin-charge-parity I-PC= 0 - + ,in contrast with the incident photon, which has J-P 1- -. This is not the case for other mesons studied at JLab, such as vector mesons, I-PC= 0 - e.g. the rho, omega, phi, for which which I-CP= 1- -, the same as for the photons. I believe this was first pointed out Ahmad, Goldstein, Liutti (arXiv:0805.3568). Here is a quote from their intro. "... deeply virtual π^0 (as well as η , η') production off a proton target is clearly distinct from the other types of meson production processes in that it involves the transition of a (virtual) photon with JPC = 1- to a JPC = 0-+ state (i.e. the final π^0 or η , η') requiring odd C-parity and

chiral odd t-channel quantum numbers. As a consequence, in a partonic description such as the one depicted in Fig.1a, the "outgoing" and "returning" quark helicities need to be opposite to one another ...".

Peter Kroll, who works very closely this group, with Sergei Goloskokov, Marcus Diehl, et al. have published extensive theoretical calculations based on Jlab data. Gary Goldstein, Simonetta Liutti have also published on this reaction.

By the way, the other meson production channels are uniquely sensitive to other interesting aspects of nucleon structure. For example, the phi, on which F-X and Patrick are working, is very sensitive to the gluon distribution in the nucleon.

In DVCS the incident and outgoing particles are both photons $JP=1^-$. Therefore, no quark helicity flip is necessary in this "virtual Compton scattering". Therefore DVCS is primarily sensitive to non-quark spin flip - eg. $H..$ The same is true with DVMP of other vector meson, such as rho. However, since the pi0 and eta are $JP=0^-$, then the transverse photon part contributing to the overall reaction cross section can cause a transversely polarized quark helicity flip. This is contained mainly in the structure functions σ_T and σ_{TT} , which can be decomposed into the transversity GPDs - mainly $Ebar_T$ and H_T .

Also, pion and eta production can still also be accompanied by non-quark helicity flips, which would be mainly contained in the longitudinal structure functions σ_{LL} . However, various theoretical papers indicate that in our accessible region of Q^2 , σ_T and σ_{TT} dominate relative to σ_L . Experimentally, this seems to be verified from JLab data . On the other hand, theory predicts that asymptotically, σ_L will dominate. From our existing 5 GeV data, we are not anywhere near there, so our experiments at JLab are really just right for accessing these transversity distributions. But, to decompose these distributions at the level of the individual quark u d flavors, we need as much precision data over as big a range as possible of kinematics in several channels - P-pi0, N-pi0, P-eta, N-eta. And, only you guys can do that! So, let me know if this makes sense to you. s a bit.

Why is Phi particularly sensitive to the phi distribution?

If you look at the proposal you will see the main diagram we are interested in has a pair of gluons from the GPD bag connecting to the hard scattering kernel that comes from the virtual photon fluctuating into a $s\bar{s}$ pair

The process you mention instead has a pair of strange quarks from the GPD bag connecting to the hard scattering kernel directly.

In practice the two processes happen. From known PDF however the gluon contribution is expected to be significantly larger than the strange quarks contribution. So the intuitive reason would be: the proton has nearly no strangeness but does have a bunch of gluons.

Now it could be that we are wrong and that the proton has more strangeness than what conventional PDF suggest. This could potentially hamper our strategy. However, intrinsic strangeness is in itself a very interesting subject, and if we did come to the conclusion that the proton has more strangeness than is conventionally accepted, then it would be a very important result.

The way I understand why the phi channel probes the gluon GPDs is because the phi meson is a strange-antistrange meson, and so doesn't interact with the up and down quarks that predominantly make up the quark content of the nucleons. This is from the phi cross section proposal: Because of its almost pure $s\bar{s}$ composition ϕ production is not affected by scattering from the nucleon's valence quarks or the light quark sea;

How to probe TMDS?

About probing TMDs, do you know exactly which groups or what channels can be used to do this at CLAS12? For example, we probe GPDs with DVCS or DVMP. Is there a similar channel that allows access to TMDs?

For first one, look for SIDIS, but I'm not sure about specific channels. I could find slides at <https://indico.cern.ch/event/568360/contributions/2487494/attachments/1438684/221358> from google, but there could be better references. I think I have seen one from collab-

oration meeting but I'm my way back from Chicago to Boston. You can find whole collaboration meeting slides at <https://www.jlab.org/indico/event/343/other-view?view=standard>

FIGURE OUT STT SLT SLL – maybe ask Paul Stoler for more information about this

Chapter 9

Thesis Goal

9.1 What do we want at the end of the day and why?

What is the Hall A DVMP measurement? gravitational form factor of the proton Why is CLAS12 particularly suited for this measurement Compare to other experiments - hall A, compass, etc. Precision estimate – 10%? 5% if we are lucky? What was precision of CLAS6? other note – intuition for process – not just getting longitudinal momentum information as with DIS, but also get the other piece of information from having put back together the proton. Read about Compton Form Factors/ extensions of. of all electrons that enter target, how many collisions do we get? probably either 1 or none? what is the probability of 1?

Very important and good starting place - write up notes from 2011 pi0 analysis note

Write to Axel at BIN Volume correction, page 75 analysis note fig 6.1

Compare integrated luminosity of CLAS6 to CLAS12 (in 2011 analysis note)

$\pi^0 \rightarrow \gamma\gamma$ branching ratio = 98.8%

Given we have an interaction, how many do we detect (ep)?

Question: Why is beam charge important? Answer (Brandon Clary, email) The accumulated beam charge is charge measured at the Faraday cup. It's important for

determining the luminosity for a run, and even being able to compare data from run to run, especially when runs may have different beam current, for example. It's just a good way to normalize to the total number of electron in that run, file, etc. In principle you could normalize by minutes, hours, etc. But beam charge, number of el., is needed to calculate the luminosity for a fixed target experiment when extracting cross sections.

Chapter 10

Analysis Scheme

10.1 Preliminary Plots

What is event rate? In Hz or in barns. What is your luminosity? Diff between Fast MC and GEMC?

10.1.1 Basic Kinematics

10.1.2 DVPP Kinematics

10.2 Technical Details

Read about kinematic fitting

10.2.1 Groovy, Python, g/Root, and more

Low t-data are very important for the meson exclusive physics. The GPD interpretation works only in the region $-t/Q^2 < 1$. From this point of view the central detector will not only increase the total statistics by a factor more than 2 but will add the valuable data with low t.

However, for pi0 the only data we have from Hall A are of very limited statistics and kinematics. One of their limitations was the relatively modest variation on

polarization parameter (epsilon) since the beam energies were not so far apart.

Number of final events in CLAS6 DVMP? About 100K, maybe 200K.

Dear Valery

CLAS12 acceptances and resolutions are also superior to that of CLAS6. Main differences are: - RGK has outbending torus vs inbending CLAS6 data - the distance between the target and the PCal has increased, the FTCal extends to lower angles, and the gap between FTCal and PCal is much smaller than between IC and EC - proton polar angle was limited to 60 deg in the e1dvcs dataset if my memory is correct

Do you have on hands the number of exclusive pi0 events published for the CLAS6 cross-sections? We need numbers to make the case to cook the RGK data

Well over an order of magnitude more statistics at CLAS12 compared to CLAS6

10.3 Proton Spin Puzzle

Puzzle Origin: How is quark contribution to proton spin measured?

10.3.1 Puzzle Origin

Do DIS with a polarized lepton on a polarized proton. The trick is to polarize the proton target in both directions, i.e. run the experiment with the target spin up and again with target spin down. Then measure the asymmetry of the scattered leptons. The EMC collaboration did this with a polarized muon simultaneously on two separate targets with opposite-sign spin. Paper is [Here](#). To measure the spin contribution of the gluons, you collide two proton beams, first with the spins aligned and then anti-aligned. This was done at RHIC a few years back (relative to 2020).

Chapter 11

Experimental Setup

11.1 Experiment Overview

11.2 Accelerator Beamline

11.2.1 Overview of Jefferson Lab

11.2.2 Electron Source

11.2.3 Polarimeters

11.2.4 Accelerator

11.2.5 Target

11.3 CEBAF Large Acceptance Spectrometer

11.3.1 Forward Detector

11.3.2 Central Detector

11.4 Experiment Running and Data Taking

Chapter 12

Simulations

12.1 Simulation Infrastructure

12.1.1 Motivation for massive simulations

12.1.2 OSG, MIT Tier 2, submission pipeline

12.2 Generator Details

12.2.1 AAO

12.2.2 AAONORAD

12.2.3 AAORAD

12.3 Simulation Pipeline

12.4 GEMC

12.5 Investigation into Simulation Speedup: Normalizing Flows

Chapter 13

Cross Section Measurement

13.1 General Analysis Overview

13.2 Data Pre-Processing

13.2.1 Energy Loss Corrections

13.2.2 Momentum Corrections

13.2.3 Simulation:Experiment Resolution Matching

Kinematics Correction of Experimental Data

Smearing Simulated Data

13.3 Particle Identification

13.4 Event Selection

13.4.1 Rigid Event Selection

13.4.2 Classifier Based Event Selection

13.5 Luminosity

13.6 Configuration and Kinematics

Chapter 14

Further Analysis

14.1 Structure Function Extraction

14.2 Comparison with CLAS6 Data

14.3 T dependence of Slope

14.4 Rosenbluth Separation Between Beam Energies

14.5 Nonparametric Methods: OMNIFOLD

14.6 Conclusion

References

Bedlinskiy, I., Kubarovskiy, V., Niccolai, S., Stoler, P., Adhikari, K. P., Anderson, M. D., ... Zonta, I. (2014). Exclusive π^0 electroproduction at $w > 2$ gev with clas. *Physical Review C - Nuclear Physics*, 90. Retrieved from <https://arxiv.org/pdf/1405.0988.pdf> doi: 10.1103/PhysRevC.90.025205

Appendix A

A.1 Full Cross Section Data

To be completed

Appendix B

B.1 Cross check between Andrey Kim and Bobby Johnston

As an additional cross check, Bobby calculated a $DV\pi^0P$ beam spin asymmetry and compared to Andrey Kim's results. This check will not comment on any acceptance, luminosity, or virtual photon flux factor calculations, but does validate exclusive event selection criteria. By examining figure B-1 we can see that agreement is reasonable, especially considering Bobby's calculation does not have sideband subtraction included.

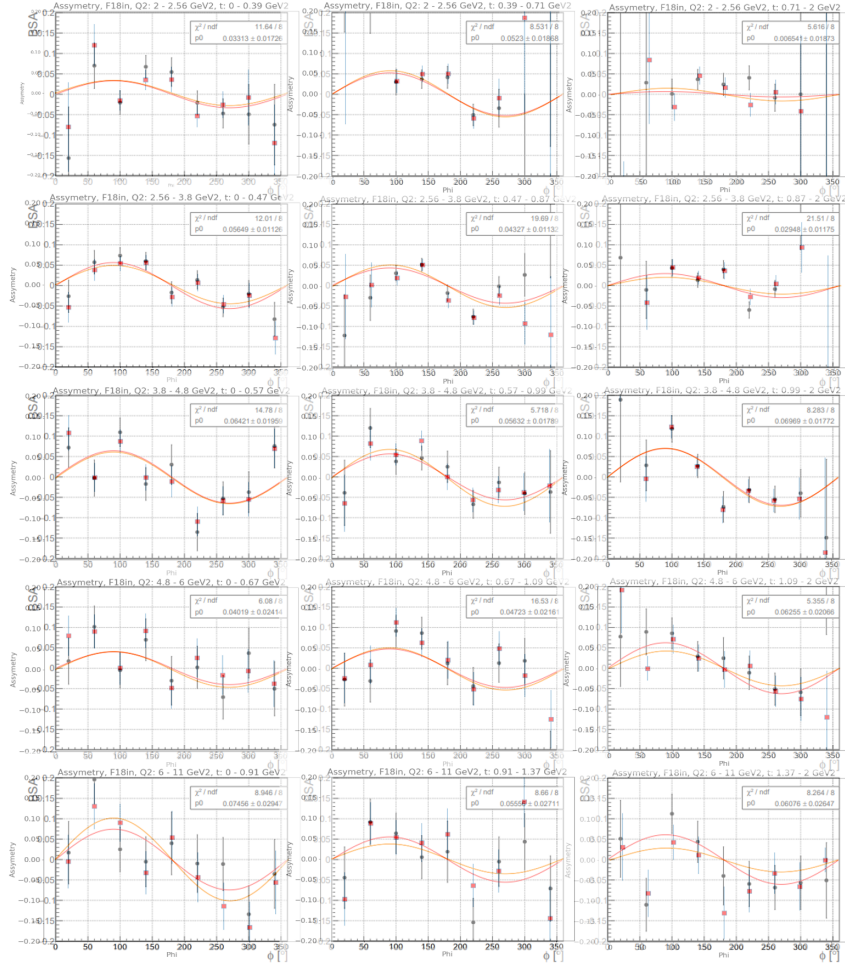


Figure B-1: Overlay comparison of Andrey Kim's results (black datapoints, red fit line) and Bobby's results (red datapoints, orange fit line).